

HANOI UNIVERSITY OF SCIENCE AND TECHNOLOGY

School of Electrical-Electronic Engineering



BACHELOR'S THESIS

COMPREHENSIVE MOTION PLANNING AND SLOSHING SUPPRESSING CONTROL FOR LIQUID TRANSPORTATION SYSTEMS

NGUYEN VIET KHANH

khanh.nv212850@sis.hust.edu.vn

Control Engineering and Automation

Supervisor: Dr. Nguyen Thi Van Anh

Supervisor's signature

Department: Automation

School: School of Electrical & Electronic Engineering

Hanoi, 6/2025

BACHELOR'S THESIS

Student name: NGUYEN VIET KHANH

Course: K66 School of Electrical & Electronics Engineering

Major: Automation and Control

- 1. Thesis title:** **Comprehensive Motion Planning And Sloshing Suppressing Control For Liquid Transportation**
- 2. Thesis content:** This thesis focus on designing a flat-based trajectory for cylindrical liquid container transporting systems using equivalent physical model to describe liquid dynamic. After that, this thesis focus on trajectory tracking control problem, obstacle avoidance and output constraint
- 3. Time of project received:** September 2024
- 4. Time of project completed:** February 2025

June 18, 2024

SUPERVISOR

Nguyen Thi Van Anh

PREFACE

I want to express my appreciation to all those who have contributed to the completion of this thesis, "Comprehensive Motion Planning And Sloshing Suppressing Control For Liquid Transportation Systems". This thesis would not have been possible without guidance and support of numerous people.

First and foremost, I give the my deepest gratitude to my academic advisor, Dr. Nguyen Thi Van Anh, for her invaluable guidance, detailed discussion and unwavering support. Also I would like to extend my hearfel to Assoc. Prof. Dr. Nguyen Tung Lam. His expertise and encouragement were instrumental in shaping the direction of this study.

I am also grateful to the faculty members of the Motion Control and Applied Robotics (MOCAR) Lab for their assistance and cooperation, especially Vu Duc Cuong and Pham Minh Duc. As graduated students, their constant steadfast support, and valuable insights have helped me to complete this study. Without their willingness to participate, this research would not have been possible. My gratitude also extends to the academic members of the School of Electrical and Electronic Engineering, whose lectures and seminars have helped me better understand the topic.

Finally, I am indebted to my family for their unending love, and support. They never stop believing in my abilities, and always prioritize my studies. Their encouragement kept me motivated, and their patience allowed me the time and space to focus on this endeavor.

Once again to sum up, completing this research has been a rewarding and instructive experience, and I really thank everyone who has contributed, directly or indirectly. I truly value your involvement at this crucial juncture in my academic career.

Sincerely

Nguyen Viet Khanh

ACKNOWLEDGEMENT

This thesis is my main research at the Department of Automation, School of Electrical Electronics Engineering, Hanoi University of Science and Technology (HUST).

In this thesis, I am the main author, propose the models, design the algorithms, writing work, and do the simulations. Besides that, I was supported by team members of the Motion Control and Applied Robotics Lab lab, and under the guide of Dr. Nguyen Thi Van Anh (HUST). Also to understand the contents of this study, the readers must be equipped with fundamental knowledge in Calculus, Algebra, Differential equations, Lagrangian and Newtonian mechanics, Linear and Nonlinear systems, ... In addition, knowledge of Robotics systems, Euler angles, Rotation matrices, and Inverse/Forward kinematics are required. It also needs a comprehensive understanding of the Lyapunov stability theory to prove the stability of Sliding Mode Control and the theory of Control Barrier Function to constraint the system output.

This study was produced by LATEX, and all of the graphs and figures were made by TikZ or properly cited. The simulations in this study are implemented in MATLAB/Simulink R2023a. The publications, which originated from this thesis and I have the role of first author/co-author, can be found on **Related publications**

SUPPLEMENTARY MATERIALS

IEEE referencing scheme is used for citations and the bibliography can be found at page 56. The equation references are placed in parentheses to distinguish them from chapter/section references.

This study is written by L^AT_EX under recover the thesis template of DATN HUST and all figures and graphs are created by TikZ or cited.

The simulations in this study are implemented in MATLAB/Simulink R2023a

The publications, which originated from this study and I have the role of author/co-author, can be found at page 51.

ABSTRACT

Liquid sloshing poses challenges across various industries where free-surface liquids can introduce unwanted dynamic effects. This phenomenon occurs when liquid inside a container oscillates due to external disturbances or changes in the container's motion. This study proposes two distinct methods to execute the liquid transfer task which considered actuator limit and output constraints. Firstly, a flatness-based trajectory planning is proposed to ensure the system performance during the transferring phase. Then, to cope with unmeasurable state variables and disturbance, an extended state observer (ESO) is integrated. In this research we proposed two different approaches for tracking control. The first one is Lyapunov-based Model Predictive Control, which integrated a Lyapunov function as a constraint. The second proposed controller approach enhances the computational efficient while having the ability to constraint the sloshing height. Integrating TSMC with Control Barrier enhances robustness against model uncertainties and disturbances while maintaining safety by constraining the maximum sloshing height. The effectiveness of the proposed control strategy is validated through numerical simulations in MATLAB/Simulink.

Keywords: Sloshing Liquid, Flat Output, Flatness-based Trajectory, Extended State Observer, Lyapunov-based Model Predictive Control, Terminal Sliding Mode Control, Control Barrier Function

TABLE OF CONTENTS

TABLE OF CONTENTS	iv
NOMENCLATURES	v
LIST OF FIGURES	viii
LIST OF TABLES	ix
1 GENERAL INTRODUCTION	1
1.1 Motivation	1
1.2 Cylindrical liquid system modeling	1
1.2.1 Numerical methods	1
1.2.2 Equivalent Mechanical Models approaches	2
1.3 Motion planning in the literature	4
1.3.1 Input command method	4
1.3.2 Optimization-based approach	4
1.3.3 Flatness-based approach	5
1.4 Controller design in related works	5
1.4.1 Feed-forward control	5
1.4.2 Feed-back control	6
1.5 Scope of the research	7
1.5.1 Reserch gap	7
1.5.2 Main contribution	7
1.5.3 Thesis structure	8
2 MODELING	9
2.1 Mathematical of cylindrical liquid container system	9
2.2 The non-flatness of the cylindrical liquid system	13
2.3 Flat output of approximate cylindrical liquid system	15
2.3.1 General case	15
2.3.2 Moving in a straight line case	17
2.3.3 Flat dynamic of cylindrical liquid system	18
2.4 Rest-to-rest trajectory	20
2.5 Time-optimal obstacle avoidance trajectory	21
3 CONTROL METHODOLOGY	23
3.1 Extended State Observer	24
3.2 Lyapunov-based Model Predictive Control	27

3.3	Terminal Sliding Mode Control with output constraint	29
3.3.1	Terminal sliding mode control	29
3.3.2	Control Barrier Function	32
4	NUMERICAL SIMULATIONS	37
4.1	Comparing different motion planning approaches	39
4.2	Trajectory Feedforward experiment	40
4.3	Controller tracking performance of time optimal trajectory	41
4.4	Sloshing height constraint for rest-to-rest trajectory	43
CONCLUSIONS		49
Related publications		51
BIBLIOGRAPHY		52

NOMENCLATURES

List of notations

a, b, c, \dots	Scalar
$\dot{a}, \dot{b}, \dot{c}, \dots$	Derivative
a_r, b_r, c_r, \dots	Reference value
$\mathbf{A}, \mathbf{a}, \mathbf{B}, \mathbf{b}, \dots$	Matrix or vector
\mathbf{A}^T	Transpose of vector \mathbf{A}
$\mathbf{0}_{m \times n}$	Zero matrix with m rows and n columns
$\mathbf{0}_m$	Zero matrix with m rows and m columns
\mathbf{I}_m	Identity matrix with m rows and m columns
$diag(a, b, c)$	Diagonal matrix
$\mathbf{A} \times \mathbf{B}$	Cross product of \mathbf{A} and \mathbf{B}
$\hat{a}, \hat{\mathbf{a}}, \dots$	Estimated values
$x[k]$	Time instance k of a varying variable x
$\mathbb{R}^{m \times n}$	Set of $m \times n$ dimensional real number
$\lambda_{\min}(\mathbf{A})$	minimum value of the eigenvalues of matrix \mathbf{A}
$\lambda_{\max}(\mathbf{A})$	maximum value of the eigenvalues of matrix \mathbf{A}
$L_f h = \nabla h^\top f$	Lie derivative
$[\dots]$	Matrix or vector
$\{ \dots \}$	Set

List of acronyms

ARE	Algebraic Riccati Equation
BIBO	Bounded Input Bounded Output
BLF	Barrier Lyapunov Function
CBF	Control Barrier Function
DoF	Degree of Freedom
ECBF	Exponential Control Barrier Function
EoM	Equation of Motion
ESO	Extended State Observer
SMC	Sliding Mode Control
TSMC	Terminal Sliding Mode Control
MPC	Model Predictive Control
LMPC	Lyapunov Model Predictive Control
LQR	Linear Quadratic Regulator
QP	Quadratic Programming

LIST OF FIGURES

Figure 1.1 Mesh used in computational domain; 14 vortex elements, 434 boundary elements, and 3326 domain elements. [1]	2
Figure 1.2 Velocity vector diagram by SPH in [4]	2
Figure 1.3 Pendulum model in [8]	3
Figure 1.4 Mass-spring-damper models from [8]	4
 Figure 2.1 Non-linear equivalent model and representation of the free surface	 9
 Figure 3.1 First control architecture for liquid sloshing in a container .	23
Figure 3.2 Second control architecture for liquid sloshing in a container	24
 Figure 4.1 Position of container	 39
Figure 4.2 Velocity of container	39
Figure 4.3 Acceleration of container	40
Figure 4.4 Sloshing height in open-loop control	40
Figure 4.5 Experimental setup	41
Figure 4.6 Displacement of container position along xy -axis - second scenario	42
Figure 4.7 Unknow disturbance for both x-axis and y-axis	42
Figure 4.8 Dislplacement of sloshing mass m_n and sloshing height \dot{q} - second scenario	43
Figure 4.9 Error of container position throughout the process in a time domain - second scenario	43
Figure 4.10 Velocity of sloshing mass m_n and velocity of container - second scenario	44
Figure 4.11 Velocity of sloshing mass m_n and velocity of container - second scenario	44
Figure 4.12 Control signal input: acceleration of container - second sce- nario	45
Figure 4.13 Error estimation of state variable \dot{q} - second scenario . . .	45
Figure 4.14 Displacement of container position along xy -axis - third sce- nario	46
Figure 4.15 Dislplacement of sloshing mass m_n and sloshing height \dot{q} - third scenario	46
Figure 4.16 Displacement of container position throughout the process in a time domain - third scenario	47

Figure 4.17 Velocity of sloshing mass m_n and velocity of container - third scenario	47
Figure 4.18 Velocity of sloshing mass m_n and velocity of container - third scenario	47
Figure 4.19 Control signal input: acceleration of container - third scenario	48
Figure 4.20 Compare controllers simulation time	48

LIST OF TABLES

Table 4.1	Parameters of the liquid sloshing system	37
Table 4.2	The performance index in second scenario	46
Table 4.3	The performance index in third scenario	48

CHAPTER 1: GENERAL INTRODUCTION

1.1 Motivation

A common occurrence in many engineering systems, such as liquid-filled industrial equipment, spacecraft, and automobile fuel tanks, is sloshing, or the dynamic motion of liquid inside a container. Because of the major issues it presents, sloshing prediction and control in these many sectors and applications require the highest attention. Uncontrolled sloshing can have serious consequences, including decreased performance, decreased stability, and possible harm to the system as a whole or nearby buildings. Sloshing effects have a significant effect on vehicle handling and maneuverability in the transportation sector. Sloshing-induced center of gravity fluctuations in automobile gasoline tanks can negatively impact vehicle dynamics, compromising fuel economy and posing safety risks. Comparably, in the aerospace field, sloshing in rocket fuel tanks can cause instability during launch and maneuvers while in orbit. These instabilities seriously compromise crew safety in addition to endangering the mission's success. Additionally, sloshing significantly affects industrial equipment that holds liquids, such as oil storage tanks and chemical processing vessels. In these situations, uncontrolled sloshing can result in equipment damage, product loss, and even environmental risks.

Therefore, it is crucial to accurately forecast and effectively regulate sloshing events. Through acquiring knowledge about the behavior and dynamics of sloshing, engineers may create control systems that effectively lessen its negative impacts. The use of predictive models and simulations is essential in comprehending the behavior of sloshing under various circumstances and directing the development of resilient control systems. exact control techniques can minimize disturbances, provide stable liquid containment, and allow for exact regulation of liquid sloshing. System performance, economy, and safety may all be enhanced by actively adjusting for sloshing dynamics and tracking intended trajectories precisely. Effective sloshing management reduces the possibility of spills or leaks while maintaining the integrity of liquid containment, improving the stability and performance of several engineering systems.

The practical requirements are to transmit containers so as to prevent excessive liquid sloshing or vibrations, and also at the beginning and final positions, the sloshing height has to be suppressed to a minimum to ensure the requirements of the technological procedure.

1.2 Cylindrical liquid system modeling

1.2.1 Numerical methods

Finite element method (FEM) proposed [1, 2] to model the fluid–structure interaction. The multi-body dynamics and solid mechanics modules were used to model

the overall structure with a hinge. The container, and the fluid inside, was moved by an input horizontal acceleration applied at the point A. The flow motion of the incompressible fluids, water and air, was modeled using laminar single phase flow module that solves the 2D Navier–Stokes equations. A negative vertical acceleration was applied to simulate the gravitational effect.

In recent years, Smoothed Particle Hydrodynamics (SPH) has emerged as a

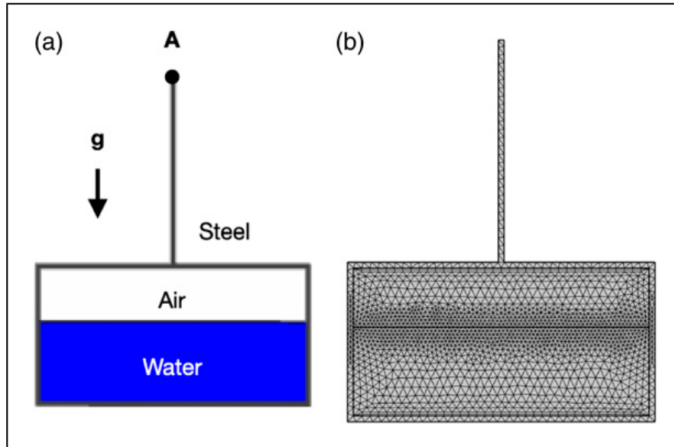


Figure 1.1: Mesh used in computational domain; 14 vortex elements, 434 boundary elements, and 3326 domain elements. [1]

promising approach for numerically simulating liquid sloshing phenomena. Its strengths lie in effectively handling large deformations, free surfaces, phase interfaces, and moving boundaries [3]. Traditional SPH techniques typically use a uniform spatial resolution (USR), but as higher accuracy and larger simulation domains are required, the computational expense grows significantly. To address this, there is a study [4] presents a numerical method based on smoothed particle hydrodynamics with adaptive spatial resolution (SPH-ASR) for liquid sloshing. The SPH-ASR method can adaptively adjust the spatial resolution based on the distance to the free surface and the moving boundary.

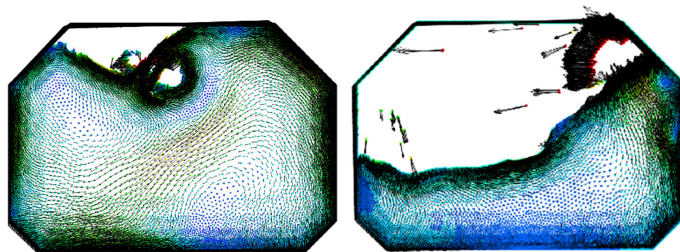


Figure 1.2: Velocity vector diagram by SPH in [4]

1.2.2 *Equivalent Mechanical Models approaches*

Traditional models commonly used in the literature to study fluid motion—such as mass-spring-damper and pendulum-based approaches. This approach offers

a computational technique for predicting the maximum sloshing height of a liquid within a container undergoing highly dynamic motion. The method strikes a balance between simplicity and accuracy—avoiding the need for physical experiments or real-system measurements, and eliminating the high computational cost typically associated with computationally-demanding fluid dynamic (CFD) simulations. Since Reference [5] shows that circumferential modes greater than one are always negligible, sloshing suppression consider the liquid motion via a single sloshing mode only give even more efficient in computation. Therefore, these are the method appropriate to apply model-based control methods.

Based on [5], some studies attempt to estimate sloshing height using basic pendulum models [6], though they often lack detail regarding the accuracy and limitations of this approach. The pendulum model can represent large slosh motions, and the spherical pendulum models are more often used to emulate nonlinear rotary sloshing [7]. However, estimating the sloshing height by means of the tangent of the pendulum angles may lead to singularity conditions when the container acceleration is high, since in this case these angles can approach 90^0 and the tangent tends to assume unrealistic high values. It is shown that the maximum accelerations for the validity of this model are between 1.2 m/s^2 and 2.3 m/s^2 .

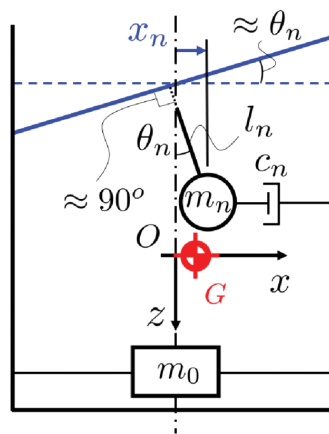


Figure 1.3: Pendulum model in [8]

A more novel approach, based on the mass–spring–damper model, is proposed in [8] for the sloshing-height estimation. Then this research direction has been studied further in [9]. This model can be exploited for assessment or optimization purposes. Experiments performed with a robot following different paths are described and also comparisons between experimental results and model predictions are very accurate compared to pendulum models. It is fairly precise for container accelerations up to (roughly) 10 m/s^2 . Based on its advantage, this model is used in this thesis.

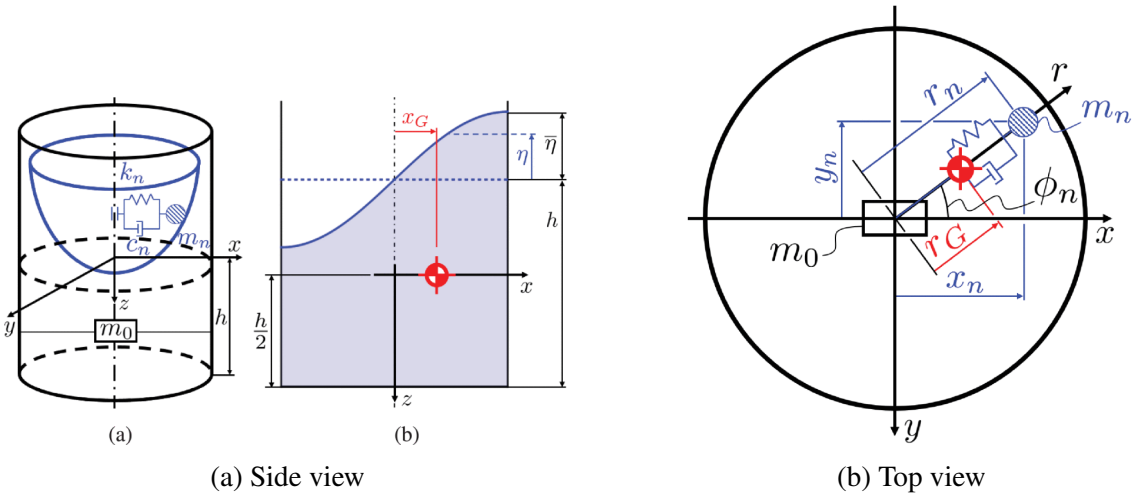


Figure 1.4: Mass-spring-damper models from [8]

1.3 Motion planning in the literature

1.3.1 Input command method

References [10, 6] suggest using input-shaping techniques, which involve peak-like inputs at specific time intervals, to cancel residual oscillations and suppress sloshing during liquid container movement. For vibration suppression, input filtering methods such as the ZVD (Zero Vibration Derivative) filter are commonly used, acting as notch filters. In [1], a robust input command is proposed, consisting of multiple steps, to eliminate residual vibrations in a multimode linear system. The step magnitudes in the shaped command are determined using only the system's resonant frequencies. The duration of the command is adjustable, allowing for the design of an optimal command that balances the reduction in transient vibrations, improvements in command robustness, and the increase in overall maneuver time.

1.3.2 Optimization-based approach

Numerous studies have explored optimization-based methods for generating motion trajectories and solving optimal control problems aimed at achieving rapid rest-to-rest transitions with minimal liquid sloshing. These methods vary widely in terms of sloshing model accuracy and optimization strategies, yet they all revolve around minimizing a cost function that accounts for the relative motion between the liquid and container.

In [11], minimum-time and minimum-energy trajectories are explored for a single-mode slosh model, revealing that while time-optimal solutions are sensitive to modeling inaccuracies, energy-optimal ones are more robust due to their extended duration. For systems where the container is underactuated, [12] proposes an iterative Riccati-based optimal controller, refined through successive linearization of the nonlinear plant. Meanwhile, [13] introduces a novel control strategy by modeling the container as if mounted on a spherical pendulum. By using the pivot's acceleration as a virtual input and applying quadratic programming, the method pro-

duces smooth, efficient transfer motions with minimal sloshing. This approach is also adopted and enhanced in this thesis. Notably, in [14], a nonlinear mass-spring-damper model is utilized as a predictive tool for constrained optimization. The study focuses on planning time-optimal trajectories for an industrial robot transporting a cylindrical container partially filled with liquid, while enforcing sloshing constraints during 1D and 2D planar movements of the container. This approach leads to low sloshing and is adopted and extended in this thesis.

1.3.3 *Flatness-based approach*

A foundational reference in this field is [15], which introduces differential flatness as a powerful tool for addressing nonlinear control problems. It includes examples such as the control of a gantry crane, where rest-to-rest motion planning becomes straightforward once a flat output is known. This concept is expanded in the study [16] to achieve rest-to-rest maneuvers for the virtual pendulum system.

For the mass-spring-damper model, there is a only study [17] that suggests a flat output for the mass-spring-damper linear model, yet there is no evidence in the literature that the flatness-based method nonlinear mass-spring-damper can be applied successfully until [18, 19]. Inspired by [17], the authour proposes approximate flat outputs within nonlinear models of sloshing liquids while also identifying key factors and evaluating their influence to address the practical issue. By using the flat output variables, a time optimal trajectory can be generated by numerical methods.

1.4 Controller design in related works

1.4.1 *Feed-forward control*

Input shaping has emerged as a potential solution for controlling liquid sloshing. This method works by generating a desired control signal with a series of pulses, resulting in a new control signal that minimizes residual vibrations. In [10], the effectiveness of this method was experimentally verified and this method has various solutions that can be applied to specific situations for velocity optimization or vibration optimization. However, all of these studies employ feed-forward control laws without feedback control loops. This can lead to inaccuracies in controlling fluid sloshing when the objective is to move the container from a starting point to an endpoint.

In recent years, there have been many research papers on seeking the flat output of the system, as the flatness property has been proven to be a strong tool for computing and controlling nonlinear systems [20, 21, 15]. In [16] introduces an advanced feed-forward control method to suppress sloshing in high-speed liquid container transfers for robotic systems. It combines a virtual pendulum tray to reduce sloshing by moving only the virtual pivot, a geometric condition to suppress specific sloshing modes, and an analytic feed-forward trajectory control based on differential flatness to design efficient rest-to-rest transport maneuvers.

The proposed control law is computationally simple and effectively eliminates higher-mode sloshing.

1.4.2 Feed-back control

There are mismatches between the actual plant and the mathematical model due to the discrete equivalent model, the complex dynamics of water, and other uncertainties. The Sliding Mode Control (SMC) technique is one such approach to robust control controller design that ensures required performance levels despite such variations [22] [23]. Additionally, SMC has been used with the generic design approach under investigation for a variety of system types, including nonlinear sloshing systems [24]. Especially when combined with the Extended State Observer (ESO). It is among the most well-known and robust control techniques for uncertain nonlinear systems. Several system types have benefited from the extensive development and use of this sophisticated method; see, for instance, [25]. Through the combination of Control Barrier Function (CBF) and Quadratic Programming (QP) [26], this methodology may be easily applied to a variety of controller types. One of the most important benefits of using CBF is that it may produce a control signal that maintains intended behavior and system stability while still adhering to predetermined output restrictions. The combination of Sliding Mode Control, Extended State Observer have been successfully applied for liquid sloshing system in [19].

For advance control method, the author has proposed Lyapunov-based Model Predictive Control for tracking trajectory and constraint the liquid sloshing height [18]. This controller has the combination between unique capacity to maintain system constraints and prediction while ensure stability and resilience of the traditional SMC . In [27] presents an Optimal Fuzzy Sliding Mode (OFSM) controller designed to manage fuel sloshing in spacecraft during orbital maneuvers. The controller's gains are optimized using a Particle Swarm Optimization (PSO) algorithm, and a novel gain scheduling approach is developed for the coupled spacecraft-fuel system. The fuzzy gains are dynamically produced based on system variables and sliding surface saturation functions. In [28] presents a new approach to reducing liquid sloshing and uncertainty in container systems, particularly in dynamic environments such as aerospace and high-speed industries. The research applies an adaptive robust wavelet control technique to handle the coupling of dynamic slosh and uncertainties from sensors or dampers, which is typically a highly nonlinear system. By developing a mathematical model for the nonlinear slosh and uncertainty, the paper uses wavelet transform to compute optimal motion that minimizes residual slosh and uncertainty.

1.5 Scope of the research

1.5.1 Research gap

- Flatness-based trajectory planning offers an efficient alternative that leverages system dynamics to derive simple control laws. These can be used to generate rest-to-rest trajectories or solve time-optimal trajectory problems more effectively, especially in complex environments. While nonlinear mass-spring-damper equivalent model show its potential to predict the cylindrical liquid dynamic. However, to the best of the author's knowledge, a flatness-based trajectory design for the mass-spring-damper model that addresses sloshing constraints has yet to be explored.
- Most existing studies on anti-sloshing primarily focus on suppressing liquid motion at the final state of the maneuver. However, during rapid acceleration, the sloshing height can become so significant that the liquid may spill out of the container entirely. For feedback control, the author recognizes that explicit constraints on sloshing height should be taken into account and further investigated.
- A comprehensive control architecture for cylindrical liquid container systems remains under explored. While individual strategies such as motion planning or feedback control have been studied extensively, an integrated framework that combines both remains limited. Such a unified approach could significantly enhance system performance by leveraging trajectory planning for anticipatory motion shaping and feedback control for real-time correction under disturbances and uncertainties. In particular, motion planning can proactively minimize sloshing by optimizing the container path, while feedback control can ensure robust stability and constraint satisfaction, especially under modeling errors or external disturbances. Studying this combined architecture is crucial for applications requiring fast and precise liquid transport, where both performance and safety (e.g., slosh height limits) must be maintained throughout the entire maneuver.

1.5.2 Main contribution

To fill in the gap, this thesis builds upon my previous work [18, 19], consolidating and presenting the core contributions from those studies in a structured manner.

- This study introduces, the flatness characterization of the approximate sloshing model. It then develops a flatness-based trajectory planning method aimed at improving system performance and reducing sloshing effects. Two different strategies—rest-to-rest interpolation and time optimization—are proposed to generate these flat-based trajectories.

- The Extended State Observer (ESO) is used to estimate combined disturbances and model uncertainties. It also provides necessary state information for controlling the liquid system, which might not be directly accessible through sensors.
- The Lyapunov-based Model Predictive Control (LMPC) approach, introduced in [26], integrates concepts from both MPC and SMC. This method not only guarantees accurate trajectory tracking and control signal convergence but also enables the handling of complex systems with multiple constraints, offering a more robust and efficient control strategy.
- The second proposed controller approach enhance the computational efficiency while having the ability to constraint the sloshing height. Integrating TSMC with Control Barrier Functions (CBF) enhances robustness against model uncertainties and disturbances while maintaining safety by constraining the maximum sloshing height. The barrier function is carefully analyzed to ensure these constraints are upheld, even in the presence of estimation errors.

1.5.3 Thesis structure

- **Chapter 1 General Introduction:** state the problem, summarize the published works, and then give the proposed plan of the thesis to solve the problem.
- **Chapter 2 Mathematical Model:** present the equivalent discrete liquid sloshing non-linear mass-spring-damper model, introduce the flat output of the system; sloshing suppression problem is considered as a flatness-based trajectory planning problems.
- **Chapter 3 Control Methodology:** Introduce the control algorithms, which includes ESO observer for estimate the lumped disturbances/uncertainties and unmeasured states, then Lyapunov-based Model Predictive Control, SMC controller and safety control CBF are introduced respectively.
- **Chapter 4 Numerical Simulation:** The effectiveness of the proposed approaches is shown through numerical simulations and comparisons.
- **Conclusion:** Conclude results and suggestions for future developments are given.

CHAPTER 2: MODELING

Modeling objective: Chapter 2 introduces the Equation of Motion (EoM) of cylindrical liquid sloshing system. Since all the proposed control methods in this thesis are model-based approach, therefore this would be the mathematical model that everything are build on. Also, in this section the approximate flat output of the system is introduced. By figuring out the approximate flat output of the system, two methods for motion planning can be applied. If we want to construct a trajectory whose final conditions do not result in a sloshing phenomenon robustly and whose computational efficiency is highly appreciated, then a rest-to-rest trajectory can be applied. This thesis also presents the geometric and quantitative constraints for more complex situations. Also, a typical method for determining reference trajectory is the optimal control approach, specifically in this study, finding the control that minimizes the total approach time to an a priori given trajectory. By representing the system in the Brunovsky form, the original nonlinear dynamics are transformed into an equivalent set of linear kinematics, which is well-suited for trajectory planning and applying desired constraints. In the time-optimal trajectory, however, the sloshing phenomenon, in which vibration remains below some tolerable level, may occur in the final position. But this problem could be overcome by the controller, which is represented in Section.

2.1 Mathematical of cylindrical liquid container system

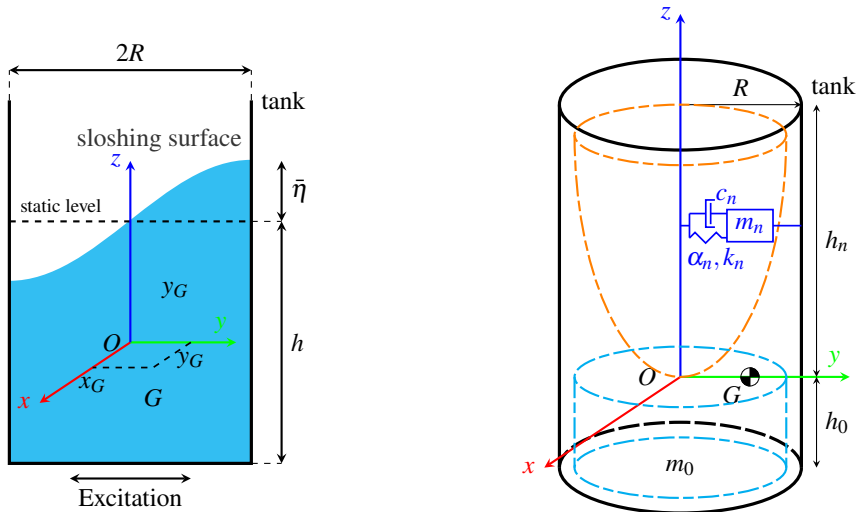


Figure 2.1: Non-linear equivalent model and representation of the free surface

In this study, our object is a cylindrical container of radius R , filled with a liquid of height h and mass m_F . There are two main components in the model, rigid mass m_0 and moving masses m_n . The overall mass of liquid calculated according to two

models must be preserved:

$$m_F = m_0 + \sum_{n=1}^{\infty} m_n \quad (2.1)$$

The n -th sloshing mass m_n can be calculated as:

$$m_n = m_F \frac{2R}{\xi_{1n} h (\xi_{1n}^2 - 1)} \tanh \left(\xi_{1n} \frac{h}{R} \right) \quad (2.2)$$

The analysis of the homogeneous response of the continuum model provides the so-called sloshing modes. To equivalent with the sloshing dynamic, each m_n is attached with a spring k_n and a damper c_n . The natural frequency for mode m_n is:

$$\omega_n^2 = \frac{g \xi_{1n}}{R} \tanh \left(\xi_{1n} \frac{h}{R} \right) \quad (2.3)$$

In Equation (2.3), (2.2) ξ_{1n} is a constant parameter known for every sloshing mode, which represents the root of the derivative of the Bessel function of the first kind concerning the radial coordinate r , for the 1st circumferential mode and the n -th radial mode, and g is the gravity acceleration. According to [29], the damping ratio can be estimated based on the liquid height h , liquid kinematic viscosity ν , and tank diameter R .

$$\zeta_n = \frac{2.89}{\pi} \sqrt{\frac{\nu}{R^{3/2} g^{1/2}}} \quad (2.4)$$

The behavior of the liquid's free surface can be categorized into three dynamic regimes, each associated with a specific model of increasing complexity. In the linear regime, the container undergoes small accelerations and mild oscillations, causing the free surface to remain approximately flat. In the weakly non-linear regime, the amplitude of oscillation becomes significant and approaches the system's natural frequencies, resulting in a distorted surface shape and the emergence of rotary sloshing effects. Finally, in the strongly non-linear regime, the free surface is subjected to extreme accelerations and strong impacts against the container walls.

In packaging applications, the strongly non-linear case is both rare and too complex for practical use. Meanwhile, the linear regime is well-understood and commonly used in industrial settings. Consequently, this study focuses on the intermediate, weakly non-linear regime to enable a more refined analysis. In this situation, the sloshing mass m_n moving along a parabolic surface, with an attached nonlinear spring exerts forces $\alpha_n k_n x_n^{2w-1}$ and $\alpha_n k_n y_n^{2w-1}$ in the x and y direction respectively and $\alpha_n k_n r_n^{2w-1}$ in the radial direction in the radial generalized coordinate r_n . The parabolic surface's analytical formula is given as follows:

$$z_n = \frac{\omega_n^2}{2g} (x_n^2 + y_n^2) \quad (2.5)$$

Take the time derivative of Equation :

$$\dot{z}_n = \frac{\omega_n^2}{g} (x_n \dot{x}_n + y_n \dot{y}_n) \quad (2.6)$$

We use the Euler-Lagrange Equation to obtain the equation of motion:

$$\begin{cases} \frac{d}{dt} \left(\frac{\partial \mathcal{T}}{\partial \dot{x}_n} - \frac{\partial \mathcal{V}}{\partial \dot{x}_n} \right) - \frac{\partial \mathcal{T}}{\partial x_n} + \frac{\partial \mathcal{V}}{\partial x_n} = -\frac{\partial \mathcal{D}}{\partial \dot{x}_n} \\ \frac{d}{dt} \left(\frac{\partial \mathcal{T}}{\partial \dot{y}_n} - \frac{\partial \mathcal{V}}{\partial \dot{y}_n} \right) - \frac{\partial \mathcal{T}}{\partial y_n} + \frac{\partial \mathcal{V}}{\partial y_n} = -\frac{\partial \mathcal{D}}{\partial \dot{y}_n} \end{cases} \quad (2.7)$$

where:

\mathcal{T} is the kinetic energy of the n -th sloshing mass, computed by its velocity $[\dot{x}_n \dot{y}_n \dot{z}_n]^T$ and $[\dot{x}_0 \dot{y}_0]^T$:

$$\begin{aligned} \mathcal{T} &= \frac{1}{2} m_n [(\dot{x}_0 + \dot{x}_n)^2 + (\dot{y}_0 + \dot{y}_n)^2 + \dot{z}_n^2] \\ &= \frac{1}{2} m_n \left[(\dot{x}_0 + \dot{x}_n)^2 + (\dot{y}_0 + \dot{y}_n)^2 + \frac{\omega_n^4}{g^2} (x_n \dot{x}_n + y_n \dot{y}_n) \right] \end{aligned} \quad (2.8)$$

\mathcal{V} is the potential energy considers the contribution of gravity and the non-linear-spring:

$$\mathcal{V} = mg z_n + \int_0^{r_n} \alpha_n k_n r_n^{2w-1} dr_n = mg \frac{\omega_n^2}{2g} (x_n^2 + y_n^2) + \frac{\alpha_n k_n}{2w} (x_n^2 + y_n^2)^w \quad (2.9)$$

\mathcal{D} is the Rayleigh function that accounts for energy dissipation:

$$\mathcal{D} = \frac{1}{2} c_n (\dot{x}_n^2 + \dot{y}_n^2 + \dot{z}_n^2) = m_n \zeta_n \omega_n \left[\dot{x}_n^2 + \dot{y}_n^2 + \frac{\omega_n^2}{g} (x_n \dot{x}_n + y_n \dot{y}_n) \right] \quad (2.10)$$

Expand (2.7) with above \mathcal{T} , \mathcal{V} and \mathcal{D} functions, setting $\beta = \frac{\omega_n^4}{g^2}$, we obtain 2 coupled EOMs for the NL model:

$$\begin{cases} (1 + \beta x_n^2) \ddot{x}_n + \beta x_n y_n \dot{y}_n + (2w_n \zeta_n (1 + \beta x_n^2) + \beta x_n \dot{x}_n) \dot{x}_n \\ + (2w_n \zeta_n \beta x_n y_n + \beta x_n \dot{y}_n) \dot{y}_n + w_n^2 x_n \left(1 + \frac{\alpha_n}{R^2} (x_n^2 + y_n^2) \right) = -\ddot{x}_0 \\ \beta x_n y_n \ddot{x}_n + (1 + \beta y_n^2) \ddot{y}_n + (2w_n \zeta_n \beta x_n y_n + \beta y_n \dot{x}_n) \dot{x}_n \\ + (2w_n \zeta_n (1 + \beta y_n^2) + \beta y_n \dot{y}_n) \dot{y}_n + w_n^2 y_n \left(1 + \frac{\alpha_n}{R^2} (x_n^2 + y_n^2) \right) = -\ddot{y}_0 \end{cases} \quad (2.11)$$

Remark 1. The first and second equation in (2.11) represents the oscillation of the moving mass m_n along the x -axis and y -axis, the left side are the accelerations that is applied to the tank respectively. Simultaneously, the similar component between two equations, interleaved by x_n , y_n , and their higher derivatives describes the impact of one direction to another, also called: the phenomenon of rotary sloshing.

For the nonlinear model, if we consider the x -axis, according to [30], using coordinate conversion from Cartesian coordinates (x, y) to polar coordinates (r, θ) , the free surface shape $\eta(r, \theta)$ is obtained by the below equation with :

$$\eta(r, \theta) = \sum_{n=1}^{\infty} \bar{\eta}_n \frac{J_1\left(\xi_{1n} \frac{r}{R}\right)}{J_1(\xi_{1n})} \cos(\theta) \quad (2.12)$$

To generalize, it is reasonable to assume that the liquid is oscillating in an arbitrary direction, which forms an angle $\theta_n = \arctan\left(\frac{y_n}{x_n}\right)$. Turning to the 2D case and shifting the r -axis to the general polar coordinate, the equation (Eq. 2.12) can be rewritten:

$$\eta(r, \theta) = \sum_{n=1}^{\infty} \bar{\eta}_n \frac{J_1\left(\xi_{1n} \frac{r}{R}\right)}{J_1(\xi_{1n})} \cos(\theta - \theta_n) \quad (2.13)$$

J_1 is the Bessel function of order 1. According to the study [31], setting $r_n = \sqrt{x_n^2 + y_n^2}$ in the polar coordinates, then the conservation of the center of gravity radial coordinate r_G

$$r_G m_F = \sum_{n=1}^{\infty} r_n m_n \quad (2.14)$$

Considering a cylindrical container filled with a liquid of height h , then r_G could be computed as:

$$\begin{aligned} r_G &= \frac{1}{\pi R^2 h} \int_0^R \int_0^{2\pi} \int_{-\frac{h}{2}}^{\frac{h}{2} + \eta(r, \theta, \bar{\eta}_n)} r^2 \cos(\theta - \theta_n) dz d\theta dr \\ &= \frac{1}{\pi R^2 h} \int_0^R \int_0^{2\pi} \int_{-\frac{h}{2}}^{\frac{h}{2} + \sum_{n=1}^{\infty} \bar{\eta}_n \frac{J_1(\xi_{1n} \frac{r}{R})}{J_1(\xi_{1n})} \cos(\theta - \theta_n)} r^2 \cos(\theta - \theta_n) dz d\theta dr = \frac{R}{h} \sum_{n=1}^{\infty} \frac{\bar{\eta}_n}{\xi_{1n}^2} \end{aligned} \quad (2.15)$$

Then the formulation of the n -th maximum sloshing height is given by:

$$\bar{\eta}_n = \frac{\xi_{1n}^2 h m_n}{m_F R} r_n = \frac{\xi_{1n}^2 h m_n}{m_F R} \sqrt{x_n^2 + y_n^2} \quad (2.16)$$

Set two specific points in the surface which are the sloshing height at the wall container:

$$\begin{aligned} \eta_x &= \eta(R, 0) = \sum_{n=1}^{\infty} \bar{\eta}_n \cos(\theta_n) \\ \eta_y &= \eta\left(R, \frac{\pi}{2}\right) = \sum_{n=1}^{\infty} \bar{\eta}_n \cos\left(\frac{\pi}{2} - \theta_n\right) = \sum_{n=1}^{\infty} \bar{\eta}_n \sin(\theta_n) \end{aligned} \quad (2.17)$$

Only consider $n = 1$, replacing the components in (Eq. 2.17) with (Eq. 2.16), we obtain

$$\begin{aligned} \eta_x &= \sum_{n=1}^{\infty} \frac{\xi_{1n}^2 h m_n}{m_F R} r_n \cos(\theta_n) = \sum_{n=1}^{\infty} \frac{\xi_{1n}^2 h m_n}{m_F R} x_n \\ \eta_y &= \sum_{n=1}^{\infty} \frac{\xi_{1n}^2 h m_n}{m_F R} r_n \sin(\theta_n) = \sum_{n=1}^{\infty} \frac{\xi_{1n}^2 h m_n}{m_F R} y_n \end{aligned} \quad (2.18)$$

Since the higher sloshing masses m_n rapidly drop for modes greater than one, the total sum of sloshing heights of these modes is negligible.

Remark 2. *This thesis only considers the first sloshing mode $n = 1$ for the sake of simplicity. Contributions of other modes can be deemed as disturbances [5]. These above equations show the output sloshing height of the system at the two mentioned points is proportional to imaginary displacements x_n and y_n of sloshing mass.*

The position of the liquid container across the (x_0, y_0) plane can be calculated by solving the aforementioned Equations of Motion. The input of the sloshing system is the external acceleration applied to the x and y axes. The ideal dynamic equation of the sloshing model can be formulated in the matrix

$$\mathbf{M}(\mathbf{q})\ddot{\mathbf{q}} + \mathbf{C}(\mathbf{q}, \dot{\mathbf{q}})\dot{\mathbf{q}} + \mathbf{G}(\mathbf{q}) = \mathbf{Ju} \quad (2.19)$$

with

$$\begin{aligned} \mathbf{M}(\mathbf{q}) &= \begin{bmatrix} m_{11} & m_{12} & 0 & 0 \\ m_{21} & m_{22} & 0 & 0 \\ 0 & 0 & 1 & 0 \\ 0 & 0 & 0 & 1 \end{bmatrix} \quad \mathbf{q} = \begin{bmatrix} x_1 \\ y_1 \\ x_0 \\ y_0 \end{bmatrix} \quad \mathbf{u} = \begin{bmatrix} u_x \\ u_y \end{bmatrix} \\ \mathbf{C}(\mathbf{q}, \dot{\mathbf{q}}) &= \begin{bmatrix} c_{11} & c_{12} & 0 & 0 \\ c_{21} & c_{22} & 0 & 0 \\ 0 & 0 & 0 & 0 \\ 0 & 0 & 0 & 0 \end{bmatrix} \quad \mathbf{G}(\mathbf{q}) = \begin{bmatrix} g_{11} \\ g_{21} \\ 0 \\ 0 \end{bmatrix} \quad \mathbf{J} = \begin{bmatrix} -\mathbf{I}_2 \\ \mathbf{I}_2 \end{bmatrix} \end{aligned}$$

$$\begin{aligned} m_{11} &= 1 + \beta x_1^2 & c_{21} &= 2\omega_n \zeta_n \beta x_1 y_1 + \beta y_1 \dot{x}_1 \\ m_{12} = m_{21} &= \beta x_1 y_1 & c_{22} &= 2\omega_n \zeta_n (1 + \beta y_1^2) + \beta y_1 \dot{y}_1 \\ m_{22} &= 1 + \beta y_1^2 & g_{11} &= \omega_n^2 x_1 \left(1 + \frac{\alpha_n}{R^2} (x_1^2 + y_1^2) \right) \\ c_{11} &= 2\omega_n \zeta_n (1 + \beta x_1^2) + \beta x_1 \dot{x}_1 & g_{21} &= \omega_n^2 y_1 \left(1 + \frac{\alpha_n}{R^2} (x_1^2 + y_1^2) \right) \\ c_{12} &= 2\omega_n \zeta_n \beta x_1 y_1 + \beta x_1 \dot{y}_1 \end{aligned}$$

2.2 The non-flatness of the cylindrical liquid system

Definition 1. According to [15], the explicit system $\dot{\mathbf{x}} = \mathbf{f}(\mathbf{x}, \mathbf{u})$ with $\mathbf{x} \in \mathbb{R}^n$, $\mathbf{u} \in \mathbb{R}^m$ is differential flat if there exists a flat output $\mathbf{y} \in \mathbb{R}^m$ in the form:

$$\mathbf{z} = \Xi \left(\mathbf{x}, \mathbf{u}, \dot{\mathbf{u}}, \dots, \mathbf{u}^{(i)} \right)$$

such that:

$$\begin{aligned} \mathbf{x} &= \Xi_x \left(\mathbf{z}, \dot{\mathbf{z}}, \dots, \mathbf{z}^{(r)} \right) \\ \mathbf{u} &= \Xi_u \left(\mathbf{z}, \dot{\mathbf{z}}, \dots, \mathbf{z}^{(r+1)} \right) \end{aligned} \quad (2.20)$$

where Ξ , Ξ_x and Ξ_u are smooth functions.

The non-flatness of the nonlinear mass-spring-damper system in 1D could be prove in any sloshing mode n^{th} . Rewrite the liquid sloshing system (Eq. 2.19) as follows:

$$\begin{cases} (1 + \beta x_n^2) \ddot{x}_n + (2\omega_n \zeta_n (1 + \beta x_n^2) + \beta x_n \dot{x}_n) \dot{x}_n \\ \quad + \omega_n^2 x_n \left(1 + \frac{\alpha}{R^2} x_n^2\right) = -\ddot{x}_0 \\ \ddot{x}_0 = u_x \end{cases} \quad (2.21)$$

To transform the system (Eq. 2.21) into the implicit system $F(\mathbf{x}, \dot{\mathbf{x}})$, we introduce an auxiliary variable

$$\begin{aligned} w_n &= \dot{x}_n + \beta x_n^2 \dot{x}_n + \dot{x}_0 \\ \dot{w}_{n0} &= (1 + \beta x_n^2) \ddot{x}_n + 2\beta x_n \dot{x}_n^2 + \ddot{x}_0 \end{aligned} \quad (2.22)$$

Considering the first equation in (Eq. 2.21), then we obtain the implicit system $F(\mathbf{x}, \dot{\mathbf{x}}) = 0$ where $\mathbf{x} = [x_n, w_n]^T$

$$\dot{w}_{n0} + 2\omega_n \zeta_n (1 + \beta x_n^2) \dot{x}_n - \beta x_n \dot{x}_n^2 + \omega_n^2 x_n \left(1 + \frac{\alpha}{R^2} x_n^2\right) = 0 \quad (2.23)$$

According to [32], we recognize the ruled manifold criterion as follows:

Theorem 1. *If System (Eq. 2.21) is flat there exists q non-zero independent vector fields g_1, \dots, g_q with $1 \leq q \leq m$, where m is the number input variables, such that*

$$F \left(\mathbf{x}, \dot{\mathbf{x}} + \sum_{j=1}^q \lambda_j \mathbf{g}_j \right) = 0 \quad (2.24)$$

for all (x, \dot{x}, \dots) in an open dense subset of \mathcal{X} , and all $\lambda = (\lambda_1, \lambda_2, \dots)$ in a neighborhood of the origin of \mathbb{R}^q . Thus, to prove that the liquid sloshing model is not flat, one could show that it is impossible to find such a nonzero \mathbf{g} vector.

PROOF. By application of Theorem 1, we could prove that the liquid sloshing model is not flat. Denote $\mathbf{g} = [g_x, g_w]^T$. Stemming from the fact that $F(\mathbf{x}, \dot{\mathbf{x}}) = 0$ and $F(\mathbf{x}, \dot{\mathbf{x}} + \lambda \mathbf{g}) = 0$, we have

$$\begin{aligned} (\dot{w}_{n0} + \lambda g_w) + 2\omega_n \zeta_n (1 + \beta x_n^2) (\dot{x}_n + \lambda g_x) \\ - \beta x_n (\dot{x}_n + \lambda g_x)^2 + \omega_n^2 x_n \left(1 + \frac{\alpha}{R^2} x_n^2\right) = 0 \end{aligned} \quad (2.25)$$

then

$$\begin{aligned} (\dot{w}_{n0} + 2\omega_n \zeta_n (1 + \beta x_n^2) \dot{x}_n - \beta x_n \dot{x}_n^2 \\ + \omega_n^2 x_n \left(1 + \frac{\alpha}{R^2} x_n^2\right)) \\ + \lambda (g_w + 2\omega_n \zeta_n (1 + \beta x_n^2) g_x - 2\beta x_n \dot{x}_n g_x) \\ - \lambda^2 (\beta x_n g_x^2) = 0 \end{aligned} \quad (2.26)$$

Since the 0th-order term is equal to zero according to (Eq. 2.23), we get the following second-degree polynomial with respect to λ

$$\lambda (g_w + 2\omega_n \zeta_n (1 + \beta x_n^2) g_x - 2\beta x_n \dot{x}_n g_x) - \lambda^2 (\beta x_n g_x^2) = 0 \quad (2.27)$$

Thus the coefficients of λ^2 and λ have to vanish identically, i.e. $g_x = 0$ and thus $g_w = 0$. Therefore, there exists no vector different from 0 such that $F(\mathbf{x}, \dot{\mathbf{x}} + \lambda \mathbf{g}) = 0$ is satisfied for all $\lambda \in \mathbb{R}$, which proves that the ruled manifold criterion is not satisfied. Hence the sloshing liquid system is not flat.

2.3 Flat output of approximate cylindrical liquid system

2.3.1 General case

From (Eq. 2.19), we can rewrite the liquid sloshing model as follows:

$$\begin{cases} (\ddot{x}_1 + 2\omega_1 \zeta_1 \dot{x}_1 + \omega_1^2 x_1) + \beta \left(\frac{1}{2} x_1^2 \ddot{x}_1 + \omega_1 \zeta_1 x_1^2 \dot{x}_1 + x_1 \dot{x}_1^2 + \frac{1}{6} \omega_1^2 x_1^3 \right) + d_{x1} = -\ddot{x}_0 \\ (\ddot{y}_1 + 2\omega_1 \zeta_1 \dot{y}_1 + \omega_1^2 y_1) + \beta \left(\frac{1}{2} y_1^2 \ddot{y}_1 + \omega_1 \zeta_1 y_1^2 \dot{y}_1 + y_1 \dot{y}_1^2 + \frac{1}{6} \omega_1^2 y_1^3 \right) + d_{y1} = -\ddot{y}_0 \\ \ddot{x}_0 = u_x \\ \ddot{y}_0 = u_y \end{cases} \quad (2.28)$$

Where the term d_{x1} and d_{y1} contain the inertial cross-coupling terms, and small nonlinear terms which are difficult to handle

$$\begin{aligned} d_{x1} &= \beta x_1 \left(y_1 \ddot{y}_1 + \dot{y}_1^2 + 2\omega_1 \zeta_1 y_1 \dot{y}_1 + \omega_1^2 \frac{\alpha_1}{\beta R^2} y_1^2 \right) \\ &\quad + \omega_1^2 \left(\frac{\alpha_1}{R^2} - \frac{\beta}{6} \right) x_1^3 + \frac{1}{2} \beta x_1^2 \ddot{x}_1 + \frac{1}{2} \omega_1 \zeta_1 x_1^2 \dot{x}_1 \\ d_{y1} &= \beta y_1 \left(x_1 \ddot{x}_1 + \dot{x}_1^2 + 2\omega_1 \zeta_1 x_1 \dot{x}_1 + \omega_1^2 \frac{\alpha_1}{\beta R^2} x_1^2 \right) \\ &\quad + \omega_1^2 \left(\frac{\alpha_1}{R^2} - \frac{\beta}{6} \right) y_1^3 + \frac{1}{2} \beta y_1^2 \ddot{y}_1 + \frac{1}{2} \omega_1 \zeta_1 y_1^2 \dot{y}_1 \end{aligned} \quad (2.29)$$

We consider $\|x_1\| \leq \varepsilon \rightarrow 0$ and $\|y_1\| \leq \varepsilon \rightarrow 0$. Assume the derivatives \dot{x}_1 , \dot{y}_1 , \ddot{x}_1 , and \ddot{y}_1 are bounded in a neighborhood of the origin; i.e., there exist constants $M_1, M_2, M_3, M_4 > 0$ and $\varepsilon_0 > 0$ such that for all $0 < \varepsilon < \varepsilon_0$:

$$|\dot{x}_1| \leq M_1, \quad |\dot{y}_1| \leq M_2, \quad |\ddot{x}_1| \leq M_3, \quad |\ddot{y}_1| \leq M_4. \quad (2.30)$$

Then, all terms in the expressions for d_{x1} and d_{y1} are bounded by functions proportional to ε , ε^2 , or ε^3 . Therefore, we conclude:

$$d_{x1} = \mathcal{O}(\varepsilon), \quad d_{y1} = \mathcal{O}(\varepsilon), \quad \text{as } \varepsilon \rightarrow 0, \quad (2.31)$$

which implies that both d_{x1} and d_{y1} remain bounded around zero and vanish at least linearly as $\varepsilon \rightarrow 0$. Then we could ignore d_{x1} and d_{y1} term in the motion planning phase. Introduce auxiliary variable as follows:

$$\begin{aligned} v_{x1} &= x_1 + \frac{\beta}{6} x_1^3 \\ \dot{v}_{x1} &= \dot{x}_1 + \frac{1}{2} \beta x_1^2 \dot{x}_1 \\ \ddot{v}_{x1} &= \ddot{x}_1 + \beta x_1 \dot{x}_1^2 + \frac{1}{2} \beta x_1^2 \ddot{x}_1 \end{aligned} \quad (2.32)$$

and

$$\begin{aligned} v_{y1} &= y_1 + \frac{\beta}{6} y_1^3 \\ \dot{v}_{y1} &= \dot{y}_1 + \frac{1}{2} \beta x_1^2 \dot{x}_1 \\ \ddot{v}_{y1} &= \ddot{y}_1 + \beta y_1 \dot{y}_1^2 + \frac{1}{2} \beta y_1^2 \ddot{y}_1 \end{aligned} \quad (2.33)$$

Firstly, I want to confirm that two functions $v_{x1} = f(x_1)$ and $v_{y1} = f(y_1)$ are injective functions. This relationship can be verified if $f(a_1) = f(a_2)$ implies $a_1 = a_2$. Suppose $f(a_1) = f(a_2)$, that means:

$$a_1 + \frac{\beta}{6} a_1^3 = a_2 + \frac{\beta}{6} a_2^3 \quad (2.34)$$

Bring everything to one side:

$$(a_1 - a_2) + \frac{\beta}{6} (a_1 - a_2) (a_1^2 + a_1 a_2 + a_2^2) = 0 \quad (2.35)$$

Factor out $(a_1 - a_2)$:

$$(a_1 - a_2) \left(1 + \frac{\beta}{6} (a_1^2 + a_1 a_2 + a_2^2) \right) = 0 \quad (2.36)$$

Since it is easy to prove that $\left(1 + \frac{\beta}{6} (a_1^2 + a_1 a_2 + a_2^2) \right) > 0$, we can imply that $v_{x1} = f(x_1)$ and $v_{y1} = f(y_1)$ are injective functions.

Denoting $\mathbf{v}_1 = [v_{x1} \ v_{y1}]^T$, $\mathbf{q}_0 = [x_0 \ y_0]^T$ and $\mathbf{d}_1 = [d_{x1} \ d_{y1}]^T$

$$\begin{cases} \ddot{\mathbf{v}}_1 + 2\omega_1 \zeta_1 \dot{\mathbf{v}}_1 + \omega_1^2 \mathbf{v}_1 + \mathbf{d}_1 = -\mathbf{u} \\ \ddot{\mathbf{q}}_0 = \mathbf{u} \end{cases} \quad (2.37)$$

Ignoring d_{x1} and d_{y1} , we have the linear approximate sloshing system as below:

$$\begin{cases} \ddot{\mathbf{v}}_1 + 2\omega_1 \zeta_1 \dot{\mathbf{v}}_1 + \omega_1^2 \mathbf{v}_1 = -\mathbf{u} \\ \ddot{\mathbf{q}}_0 = \mathbf{u} \end{cases} \quad (2.38)$$

Remark 3. It is important to notice that the model error of (Eq. 2.38) is significantly small because one could choose the maximum sloshing height $\epsilon = \bar{\eta}_{max}$ small enough and d_n contain mainly ϵ^2 and ϵ^3 terms. In addition, the approximate model still retains nonlinear properties. As a consequence, the proposed approximate model could be applied to larger and more complicated oscillations compared to linear models. Therefore, the flat output of this approximate model could be applied in the trajectory phases for the liquid sloshing system (Eq. 2.19).

Theorem 2. By Definition 1, the flat output of the system 2.38 is:

$$\mathbf{z} = \mathbf{q}_0 - \frac{2\zeta_1}{\omega_1} \dot{\mathbf{q}}_0 + (1 - 4\zeta_1^2) \mathbf{v}_1 - 2 \frac{\zeta_1}{\omega_1} \dot{\mathbf{v}}_1 \quad (2.39)$$

all the state variable and control input could be expressed as a function of $\mathbf{z} = [z_1 \ z_2]^T$ and its higher-order derivatives.

PROOF. Taking the first time and the second derivative of the flat output

$$\begin{cases} \dot{\mathbf{z}} &= \dot{\mathbf{q}}_0 + 2\omega_1\zeta_1\mathbf{v}_1 + \dot{\mathbf{v}}_1 \\ \ddot{\mathbf{z}} &= -\omega_1^2\mathbf{v}_1 \end{cases} \quad (2.40)$$

Then we could express \mathbf{v}_1 , $\dot{\mathbf{v}}_1$ and $\ddot{\mathbf{v}}_1$ by \mathbf{y} higher-order derivative as follows

$$\begin{cases} \mathbf{v}_1 &= -\ddot{\mathbf{z}}/\omega_1^2 \\ \dot{\mathbf{v}}_1 &= -\mathbf{z}^{(3)}/\omega_1^2 \\ \ddot{\mathbf{v}}_1 &= -\mathbf{z}^{(4)}/\omega_1^2 \end{cases} \quad (2.41)$$

Using these relationships in Equation 2.41, we can imply the function of \dot{x}_0 and \ddot{y}_0 by flat output in Equation 2.40

$$\dot{\mathbf{q}}_0 = \frac{\mathbf{y}^{(3)}}{\omega_1^2} + \frac{2\zeta_1}{\omega_1}\ddot{\mathbf{y}} + \dot{\mathbf{y}} \quad (2.42)$$

Then the below function of x_0 , \dot{x}_0 , y_0 and \ddot{y}_0 can be inferred from Equations 2.39 and 2.42.

$$\begin{cases} \mathbf{q}_0 &= \frac{1}{\omega_1^2}\ddot{\mathbf{z}} + \frac{2\zeta_1}{\omega_1}\dot{\mathbf{z}} + \mathbf{z} \\ \dot{\mathbf{q}}_0 &= \frac{1}{\omega_1^2}\mathbf{z}^{(4)} + \frac{2\zeta_1}{\omega_1}\mathbf{z}^{(3)} + \ddot{\mathbf{z}} \end{cases} \quad (2.43)$$

Above are all the functions $\mathbf{x} = \Xi_{\mathbf{x}}(\mathbf{z}, \dot{\mathbf{z}}, \dots, \mathbf{z}^{(r)})$ and $\mathbf{u} = \Xi_{\mathbf{u}}(\mathbf{z}, \dot{\mathbf{z}}, \dots, \mathbf{z}^{(r+1)})$, so the condition of Definition 1 is satisfied. This is the end of the proof. Given that the system in Equation 2.38 approximates the system in Equation 2.19, the proposed flat output may serve as an approximate flat output for motion planning.

2.3.2 Moving in a straight line case

If between different processes there are no obstacles in the trajectory, the container can move in a straight line, and the phenomenon of rotary sloshing can be neglected.

$$\begin{aligned} y_1 &= \tan(\theta_1)x_1 = \alpha_x x_1 \\ \ddot{y}_0 &= \tan(\phi)\ddot{x}_0 = \alpha_x \ddot{x}_0 \end{aligned} \quad (2.44)$$

where α_x is a constant and $\phi = \theta_1$ or $\phi = \theta_1 + \pi$. Then the proposed flat output of approximate liquid sloshing system could be more accurate if we set the variable as follow $y_1 = \tan \theta_1 x_1 = \alpha_x x_1$ and $x_1 = \cot \theta_1 y_1 = \alpha_y y_1$. For simplification, we denote such as $\beta_1 = (1 + \alpha_x^2)\beta$, $\alpha_{x1} = \alpha_1(1 + \alpha_x^2)$. Without loss of generality, the problem in 2D space can be reduced to the problem in 1D space since the container is moving forward in the predetermined ϕ to each other, consider the x -axis

$$\begin{aligned} (1 + \beta x_1^2)\ddot{x}_1 + \beta \alpha_x^2 x_1^2 \ddot{x}_1 + (2\omega_1 \zeta_1 (1 + \beta x_1^2) + \beta x_1 \dot{x}_1) \dot{x}_1 \\ + (2\omega_1 \zeta_1 \beta \alpha_x x_1^2 + \beta \alpha_x x_1 \dot{x}_1) \alpha_x \dot{x}_1 + \omega_1^2 \left(1 + \frac{\alpha_1}{R^2} (x_1^2 + \alpha_x^2 x_1^2)\right) x_1 = -\ddot{x}_0 \end{aligned} \quad (2.45)$$

Transforming from the above equation, we could obtain

$$\begin{aligned} & (\ddot{x}_1 + 2\omega_1 \zeta_1 \dot{x}_1 + \omega_1^2 x_1) + \beta_1 \left(\frac{1}{2} x_1^2 \ddot{x}_1 + \omega_1 \zeta_1 x_1^2 \dot{x}_1 + x_1 \dot{x}_1^2 + \frac{1}{6} \omega_1^2 x_1^3 \right) \\ & + \omega_1^2 \left(\frac{\alpha_{x1}}{R^2} - \frac{\beta_1}{6} \right) x_1^3 + \frac{1}{2} \beta_1 x_1^2 \ddot{x}_1 + \frac{1}{2} \omega_1 \zeta_1 x_1^2 \dot{x}_1 = -\ddot{x}_0 \end{aligned} \quad (2.46)$$

setting $d_{x1} = \omega_1^2 \left(\frac{\alpha_{x1}}{R^2} - \frac{\beta_1}{6} \right) x_1^3 + \frac{1}{2} \beta_1 x_1^2 \ddot{x}_1 + \frac{1}{2} \omega_1 \zeta_1 x_1^2 \dot{x}_1$. If we consider $\|x_1\| \leq \varepsilon \rightarrow 0$ then

$$\begin{aligned} \lim_{\varepsilon \rightarrow 0} d_{x1} &= \lim_{\varepsilon \rightarrow 0} \omega_1^2 \left(\frac{\alpha_{x1}}{R^2} - \frac{\beta_1}{6} \right) \varepsilon^3 + \frac{1}{2} \beta_1 \varepsilon^2 \ddot{x}_1 + \frac{1}{2} \omega_1 \zeta_1 \varepsilon^2 \dot{x}_1 \\ &= \lim_{\varepsilon \rightarrow 0} \varepsilon^2 \left(\omega_1^2 \left(\frac{\alpha_{x1}}{R^2} - \frac{\beta_1}{6} \right) \varepsilon + \frac{1}{2} \beta_1 \ddot{x}_1 + \frac{1}{2} \omega_1 \zeta_1 \dot{x}_1 \right) = 0 \end{aligned} \quad (2.47)$$

Notice that the term ε^2 makes the error small relative to the general case. Regrouping terms in the system equation

$$\left(\ddot{x}_1 + \beta_1 x_1 \dot{x}_1^2 + \frac{1}{2} \beta_1 x_1^2 \ddot{x}_1 \right) + 2\omega_1 \zeta_1 \left(\dot{x}_1 + \frac{1}{2} \beta_1 x_1^2 \dot{x}_1 \right) + \omega_1^2 \left(x_1 + \frac{\beta_1}{6} x_1^3 \right) + d_{x1} = -\ddot{x}_0 \quad (2.48)$$

Again, if we introduce the auxiliary variable $v_{x1} = x_1 + \frac{\beta_1}{6} x_1^3$, the system would turn into

$$\begin{cases} \ddot{v}_{x1} + 2\omega_1 \zeta_1 \dot{v}_{x1} + \omega_1^2 v_{x1} + d_{x1} = -\ddot{x}_0 \\ \ddot{x}_0 = u_x \end{cases} \quad (2.49)$$

Similarly, we could prove that the above system has the flat output

$$z_1 = x_0 - \frac{2\zeta_1}{\omega_1} \dot{x}_0 + (1 - 4\zeta_1^2) v_{x1} - \frac{2\zeta_1}{\omega_1} \dot{v}_{x1} \quad (2.50)$$

The other flat output, $z_2 = \alpha_x z_1$, can be readily derived from z_1 .

Remark 4. It is important to emphasize that when the container only needs to move along a straight line, the problem becomes significantly simpler. In this case, not only is the trajectory planning error substantially reduced, but the computational burden is also lowered. Specifically, it is sufficient to compute a single flat output, z_1 , from which the second flat output, z_2 , can be directly derived using the known linear relationship $z_2 = \alpha_x z_1$. This greatly simplifies the overall control design and enhances computational efficiency.

2.3.3 Flat dynamic of cylindrical liquid system

Denote $\mathbf{x}_s = [v_{x1} \ \dot{v}_{x1} \ \ddot{v}_{x1} \ x_0 \ \dot{x}_0 \ \ddot{x}_0]^T$, $\mathbf{y}_s = [v_{y1} \ \dot{v}_{y1} \ \ddot{v}_{y1} \ y_0 \ \dot{y}_0 \ \ddot{y}_0]^T$, and the flat output as $\mathbf{z}_1 = [z_{s1} \ \dot{z}_1 \ \ddot{z}_1 \ z_1^{(3)} \ z_1^{(4)}]^T$, $\mathbf{z}_2 = [z_{s2} \ \dot{z}_2 \ \ddot{z}_2 \ z_2^{(3)} \ z_2^{(4)}]^T$, we could compute every state variable by the flat output in the matrix form

$$\begin{bmatrix} \mathbf{x}_s \\ \mathbf{y}_s \end{bmatrix} = \begin{bmatrix} \mathbf{A}_{f2s} & \mathbf{0}_{5 \times 6} \\ \mathbf{0}_{5 \times 6} & \mathbf{A}_{f2s} \end{bmatrix} \begin{bmatrix} \mathbf{z}_{s1} \\ \mathbf{z}_{s2} \end{bmatrix} \quad (2.51)$$

where

$$\mathbf{A}_{f2s} = \begin{bmatrix} 0 & 0 & -1/\omega_1^2 & 0 & 0 \\ 0 & 0 & 0 & -1/\omega_1^2 & 0 \\ 0 & 0 & 0 & 0 & -1/\omega_1^2 \\ 1 & 2\zeta_1/\omega_1 & 1/\omega_1^2 & 0 & 0 \\ 0 & 1 & 2\zeta_1/\omega_1 & 1/\omega_1^2 & 0 \\ 0 & 0 & 1 & 2\zeta_1/\omega_1 & 1/\omega_1^2 \end{bmatrix} \quad (2.52)$$

Notice that we could solve x_1 , y_1 from v_{x1} and v_{y1} by the Cubic equations 2.32 2.33. One could use table look up method or the explicit solution form of the cubic equation. Finally, the equivalent system of the one represented by equation (2.38) can be written explicitly in Brunovsky form:

$$\dot{\mathbf{z}} = \mathbf{A}_{flat}\mathbf{z} + \mathbf{B}_{flat}\mathbf{v} \quad (2.53)$$

with the state vector $\mathbf{z} = [z_1 \ z_2 \ \dot{z}_1 \ \dot{z}_2 \ \ddot{z}_1 \ \ddot{z}_2 \ z_1^{(3)} \ z_2^{(3)}]^T$ and the input vector $\mathbf{v} = [z_1^{(4)} \ z_2^{(4)}]^T$. Define other matrices as below:

$$\mathbf{A}_{flat} = \begin{bmatrix} \mathbf{0}_2 & \mathbf{I}_2 & \mathbf{0}_2 & \mathbf{0}_2 \\ \mathbf{0}_2 & \mathbf{0}_2 & \mathbf{I}_2 & \mathbf{0}_2 \\ \mathbf{0}_2 & \mathbf{0}_2 & \mathbf{0}_2 & \mathbf{I}_2 \\ \mathbf{0}_2 & \mathbf{0}_2 & \mathbf{0}_2 & \mathbf{0}_2 \end{bmatrix} \quad \mathbf{B}_{flat} = \begin{bmatrix} \mathbf{0}_2 \\ \mathbf{0}_2 \\ \mathbf{0}_2 \\ \mathbf{I}_2 \end{bmatrix} \quad (2.54)$$

The Equation 2.53 is the core of this thesis, other proposed trajectory planning methods are based on it. Therefore, it is reasonable to determine which term of it would be eliminated compared to the system in Equation 2.37. Setting $\gamma_1 = \mathbf{z}$, $\gamma_2 = \dot{\mathbf{z}}$, $\gamma_3 = \ddot{\mathbf{z}}$, and $\gamma_4 = \mathbf{z}^{(3)}$, applied for the nonlinear system in (Eq. 2.19), then we have:

$$\begin{aligned} \dot{\gamma}_1 &= \dot{\mathbf{z}} = \dot{\mathbf{q}}_0 - \frac{2\zeta_1}{\omega_1} \ddot{\mathbf{q}}_0 + (1 - 4\zeta_1^2) \dot{\mathbf{v}}_1 - 2 \frac{\zeta_1}{\omega_1} \ddot{\mathbf{v}}_1 \\ &= \dot{\mathbf{q}}_0 - \frac{2\zeta_1}{\omega_1} (-\ddot{\mathbf{v}}_1 - 2\omega_1 \zeta_1 \dot{\mathbf{v}}_1 - \omega_1^2 \mathbf{v}_1 - \mathbf{d}_1) + (1 - 4\zeta_1^2) \dot{\mathbf{v}}_1 - 2 \frac{\zeta_1}{\omega_1} \ddot{\mathbf{v}}_1 \\ &= \gamma_2 + \frac{2\zeta_1}{\omega_1} \mathbf{d}_1 \end{aligned}$$

$$\begin{aligned} \dot{\gamma}_2 &= \ddot{\mathbf{z}} = \ddot{\mathbf{q}}_0 + 2\omega_1 \zeta_1 \dot{\mathbf{v}}_1 + \ddot{\mathbf{v}}_1 \\ &= (-\ddot{\mathbf{v}}_1 - 2\omega_1 \zeta_1 \dot{\mathbf{v}}_1 - \omega_1^2 \mathbf{v}_1 - \mathbf{d}_1) + 2\omega_1 \zeta_1 \dot{\mathbf{v}}_1 + \ddot{\mathbf{v}}_1 \\ &= \gamma_3 - \mathbf{d}_1 \end{aligned}$$

In contrast, there are no error in γ_3 and γ_4 since $\dot{\gamma}_3 = \gamma_4 = -\omega_1^2 \dot{\mathbf{v}}_1$, $\dot{\gamma}_4 = \mathbf{z}^{(4)} = -\omega_1^2 \ddot{\mathbf{v}}_1 = \mathbf{v}$

Thus, the dynamic of the nonlinear system 2.37 is rewritten according to the system

of equations of the state variables $\boldsymbol{\gamma} = [\boldsymbol{\gamma}_1^T \ \boldsymbol{\gamma}_2^T \ \boldsymbol{\gamma}_3^T \ \boldsymbol{\gamma}_4^T]^T$, $\boldsymbol{d}_{\gamma} = [\boldsymbol{d}_1^T \ \boldsymbol{d}_2^T \ \mathbf{0}_{1 \times 4}]^T$ as follows:

$$\dot{\boldsymbol{\gamma}} = \mathbf{A}_{flat}\boldsymbol{\gamma} + \mathbf{B}_{flat}\boldsymbol{v} + \boldsymbol{d}_{\gamma} \quad (2.55)$$

Remark 5. Although the flat output and its higher-order derivatives are expressed in terms of different state variables, each derivative is primarily governed by a specific key state. Specifically, the flat output \mathbf{y} and its derivatives $\dot{\mathbf{z}}$, $\ddot{\mathbf{z}}$, $\mathbf{z}^{(3)}$, and $\mathbf{z}^{(4)}$ correspond to the container position \mathbf{q}_0 , container velocity $\dot{\mathbf{q}}_0$, sloshing mass position \mathbf{v}_1 , and sloshing mass velocity $\dot{\mathbf{v}}_1$, respectively.

The eliminated disturbance term \boldsymbol{d}_1 primarily contributes to errors in $\boldsymbol{\gamma}_1$ and $\boldsymbol{\gamma}_2$, which represent position and velocity. However, since the sloshing height is relatively small compared to the container's overall position, the use of the simplified Brunovsky form in Equation 2.53 is both computationally efficient and introduces an acceptable level of error for trajectory planning purposes.

2.4 Rest-to-rest trajectory

Definition 2. For the system in the Definition 1, if the initial point $x(\mathbf{x}(t_i); \mathbf{u}(t_i))$ and final point $x(\mathbf{x}(t_f); \mathbf{u}(t_f))$ are equilibrium points, we have $\dot{\mathbf{x}}(t_i) = 0$, $\dot{\mathbf{u}}(t_i) = 0$ and $\dot{\mathbf{x}}(t_f) = 0$, $\dot{\mathbf{u}}(t_f) = 0$. It is known that for the associated trivial system, $\mathbf{y}(t_i)$ and $\mathbf{y}(t_f)$ are both equilibrium points. According to [15], we possess:

$$\begin{aligned} \mathbf{x}(t_i) &= \Xi_x \left(\mathbf{z}(t_i), \dot{\mathbf{z}}(t_i) = \mathbf{0}, \dots, \mathbf{z}^{(r)}(t_i) = \mathbf{0} \right), \\ \mathbf{u}(t_i) &= \Xi_u \left(\mathbf{z}(t_i), \dot{\mathbf{z}}(t_i) = \mathbf{0}, \dots, \mathbf{z}^{(r+1)}(t_i) = \mathbf{0} \right) \\ \mathbf{x}(t_f) &= \Xi_x \left(\mathbf{z}(t_f), \dot{\mathbf{z}}(t_f) = \mathbf{0}, \dots, \mathbf{z}^{(r)}(t_f) = \mathbf{0} \right), \\ \mathbf{u}(t_f) &= \Xi_u \left(\mathbf{z}(t_f), \dot{\mathbf{z}}(t_f) = \mathbf{0}, \dots, \mathbf{z}^{(r+1)}(t_f) = \mathbf{0} \right) \end{aligned}$$

The polynomial rest-to-rest trajectories are of the form:

$$z(t) = z(t_i) + \left(\frac{t - t_i}{t_f - t_i} \right)^{r+2} \left(\sum_{k=0}^{r+1} \alpha_k \left(\frac{t - t_i}{t_f - t_i} \right)^k \right), \quad j = 1, \dots, m \quad (2.56)$$

with $[\alpha_0 \dots \alpha_{r+1}]^T = \mathbf{A}_{r2r}^{-1} \mathbf{B}_{r2r}$ where \mathbf{A}_{r2r} and \mathbf{B}_{r2r} are given by

$$\mathbf{A}_{r2r} = \begin{bmatrix} 1 & 1 & \dots & 1 \\ r+2 & r+3 & & 2r+3 \\ (r+1)(r+2) & (r+2)(r+3) & (2r+2)(2r+3) \\ \vdots & & \vdots \\ (r+2)! & \frac{(r+3)!}{2} & \dots & \frac{(2r+3)!}{(r+2)!} \end{bmatrix} \quad \mathbf{B}_{r2r} = \begin{bmatrix} 1 \\ 0 \\ \vdots \\ 0 \end{bmatrix} \quad (2.57)$$

For cylindrical liquid sloshing system, $r = 3$, and in the case of moving in the straight line, we obtain $\begin{bmatrix} \alpha_0 & \alpha_1 & \alpha_2 & \alpha_3 & \alpha_4 \end{bmatrix}^T = \begin{bmatrix} 126 & -420 & 540 & -315 & 70 \end{bmatrix}^T$, then

$$\begin{aligned} z_1 &= x_i + (x_f - x_i)(126 - 420\tau + 540\tau^2 - 315\tau^3 + 70\tau^4)\tau^5 \\ z_2 &= y_i + (y_f - y_i)(126 - 420\tau + 540\tau^2 - 315\tau^3 + 70\tau^4)\tau^5 \end{aligned} \quad (2.58)$$

where $\tau = (t - t_i) / (t_f - t_i)$. We can design a geometric path that maintains a safe distance from obstacles, and then adjust the motion along this path to achieve the desired rest-to-rest behavior. Suppose the system starts at position (x_i, y_i) at time t_i , ends at (x_f, y_f) at time t_f , and is at rest at both points. The trajectory is also required to pass through an intermediate point (x_c, y_c) , chosen as the furthest point from any obstacles along the route. As a result, the desired trajectory function $f : z_1 \rightarrow z_2$ must satisfy four specific conditions.

$$\begin{aligned} z_2(x_i) &= y_i, \quad z_2(x_f) = y_f, \\ z_2(x_c) &= y_c, \quad \frac{dz_2}{dz_1}(x_c) = 0 \end{aligned} \quad (2.59)$$

and the constraint $\frac{d^2y_0}{dx_0^2}(x_c) < 0$ to have a local maximum or minimum at this point. Denote the normalize value $z_1^{nor} = \frac{y_1 - x_i}{x_f - x_i}$ and $z_2^{nor} = \frac{y_2 - y_i}{y_f - y_i}$. Then we can construct a general 3rd-degree polynomial function of y_2 in y_1 :

$$z_2(z_1) = y_i + (y_f - y_i) z_1^{nor} (c_2(z_1^{nor})^2 + c_1 z_1^{nor} + c_0) \quad (2.60)$$

where $\mathbf{A}_{r2rcons} [c_2 \ c_1 \ c_0]^T = \mathbf{B}_{r2rcons}$, $x_c^{nor} = \frac{x_c - x_i}{x_f - x_i}$ and $y_c^{nor} = \frac{y_c - y_i}{y_f - y_i}$, given that

$$\mathbf{A}_{r2rcons} = \begin{bmatrix} 1 & 1 & 1 \\ (x_c^{nor})^2 & x_c^{nor} & 1 \\ 3(x_c^{nor})^2 & 2x_c^{nor} & 1 \end{bmatrix} \mathbf{B}_{r2rcons} = \begin{bmatrix} 1 \\ x_c^{nor} y_c^{nor} \\ 0 \end{bmatrix} \quad (2.61)$$

2.5 Time-optimal obstacle avoidance trajectory

For computational tractability, the optimized trajectory is discretized into N segments, a pre-selected constant. Hence, the sampling time t_s is:

$$t_s = \frac{T}{N} = \frac{t_f - t_i}{N} \quad (2.62)$$

where T is the time instant (to be determined) when the tank reaches the terminal state. Then, by assuming the input v to be a zero-order hold (ZOH) signal, the continuous kinematics in equation (2.53) can be discretized by:

$$\mathbf{z}(k+1) = \mathbf{A}_{flat}\mathbf{z}(k) + \mathbf{B}_{flat}\mathbf{v}(k) \quad (2.63)$$

where $\mathbf{z}(k)$ and $\mathbf{v}(k)$ are the discretized state vectors of \mathbf{z} and \mathbf{v} at the k^{th} node respectively. The subscripts v , a , j , and s represent velocity, acceleration, jerk, and snap respectively. Overall, the optimization variables are comprised of T , $\mathbf{z}(k)$ and $\mathbf{v}(k)$ for all $k \in [1, N+1] \subseteq \mathbb{N}$ of which the concatenated vector belongs to $\mathbb{R}^{(10N+1) \times 1}$. With all the constraints listed above, we can execute the optimization problem as:

$$\begin{aligned}
& \underset{t_f, \mathbf{v}(k)}{\text{minimize}} \quad J = t_f - t_i \\
& \text{subject to} \quad \mathbf{z}(k+1) = \mathbf{A}_{flat}\mathbf{z}(k) + \mathbf{B}_{flat}\mathbf{v}(k), \quad \forall k \in [1, N] \subset \mathbb{N} \\
& \quad |\bar{\eta}_n(k)| \leq \bar{\eta}_{n,\max}, \quad \forall k \in [1, N] \subset \mathbb{N} \quad (\text{Sloshing height}) \\
& \quad |\dot{\mathbf{q}}_0(k)| \leq \dot{\mathbf{q}}_{0,\max}, \quad \forall k \in [1, N] \subset \mathbb{N} \quad (\text{Velocity}) \\
& \quad |\ddot{\mathbf{q}}_0(k)| \leq \ddot{\mathbf{q}}_{0,\max}, \quad \forall k \in [1, N] \subset \mathbb{N} \quad (\text{Force}) \\
& \quad \mathbf{z}(0) = \mathbf{z}_{in}, \quad \mathbf{z}(N+1) = \mathbf{z}_f \quad (\text{Boundary conditions}) \\
& \quad \text{Rect}_i(k) \forall i \in [1, n_{rec}], \text{Cir}_j(k) \forall j \in [1, n_{cir}] \quad (\text{Geometry})
\end{aligned} \tag{2.64}$$

By adding the obstacle constraint to the optimization problem, the optimal trajectory in time and obstacle avoidance is achieved as follows:

$$\text{Rectangle}_i = \{(x, y) : s_1 \leq x \leq s_2, s_3 \leq y \leq s_4\} \quad \forall i = 1, \dots, n_{rec} \tag{2.65}$$

where n_{rec} is the number of rectangle obstacles. Then the constraint for rectangle obstacles could be described as:

$$\text{Rect}(x = x_0(k), y = y_0(k)) = \sum_{j=1}^2 \|x - s_j\| + \|y - s_{j+2}\| > \|s_1 - s_2\| + \|s_3 - s_4\| \tag{2.66}$$

Also, we could define the circle obstacle as:

$$\text{Circle}_i = \{(x, y) : (x - x_{cir})^2 + (y - y_{cir})^2 \leq r_{cir}^2\} \quad \forall i = 1, \dots, n_{cir} \tag{2.67}$$

Similarly, the constraint for circle obstacles could be described as:

$$\text{Cir}(x = x_0(k), y = y_0(k)) = (x - x_{cir})^2 + (y - y_{cir})^2 > r_{cir}^2 \tag{2.68}$$

In this work, the optimization problem Equation 2.64 is solved using the numerical optimization tool CasADi in MATLAB, with the ‘IPOPT’ solver. After we get the solution $\mathbf{z}(k) \forall k \in [1, N+1] \subseteq \mathbb{N}$, the reference trajectory could be obtain from Equation 2.51.

CHAPTER 3: CONTROL METHODOLOGY

Control objective: This chapter introduces the control methodologies developed in this work to address the challenges of liquid sloshing suppression and trajectory tracking. An ESO is proposed in (Section 3.1) for observation of the unmeasurable state variables, and the total disturbances of the liquid sloshing system by using output measurement. In the first approach, I use LMPC (Section 3.2) to tracking reference trajectory and performing output constraint. The TSMC is a nominal controller (Section 3.3) for anti-sloshing and tracking problems. Subsequently, Control Barrier Function - Quadratic Programming is introduced to ensure that the liquid sloshing system is in a safe range with a constrained maximum sloshing height (Section 3.3.2). Both controller's reference flatness-based trajectories, which are optimized for minimum transfer time and structured to avoid obstacles in a disturbed environment. These strategies collectively aim to maintain liquid stability, achieve high-speed transport, and ensure safe operation in practical applications.

disturbance.

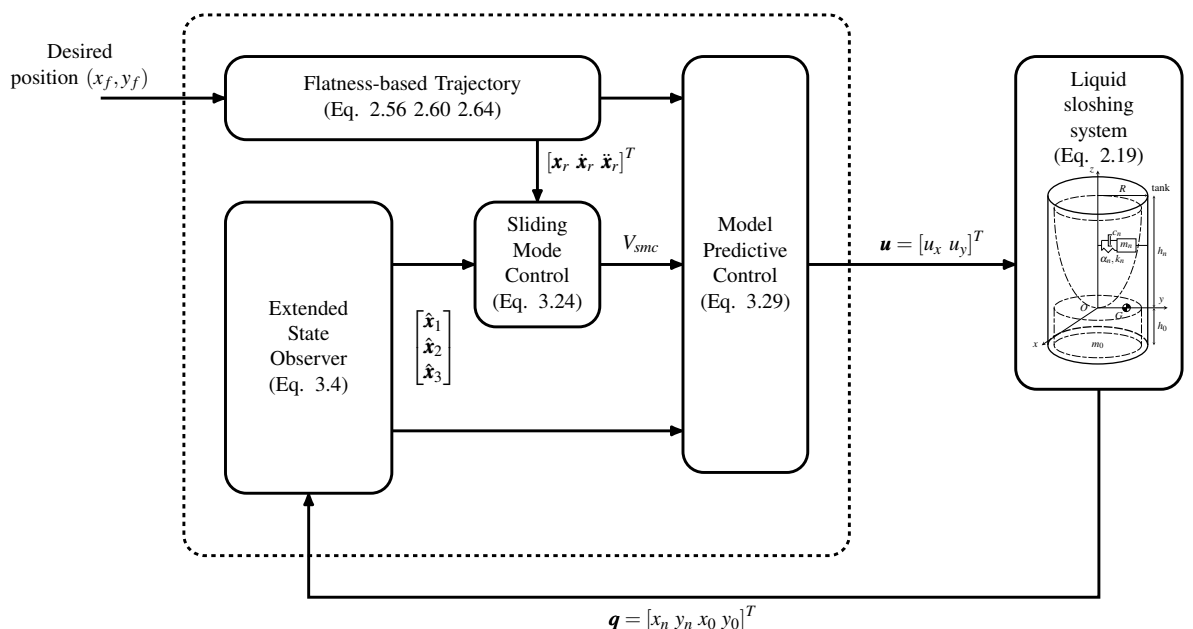


Figure 3.1: First control architecture for liquid sloshing in a container

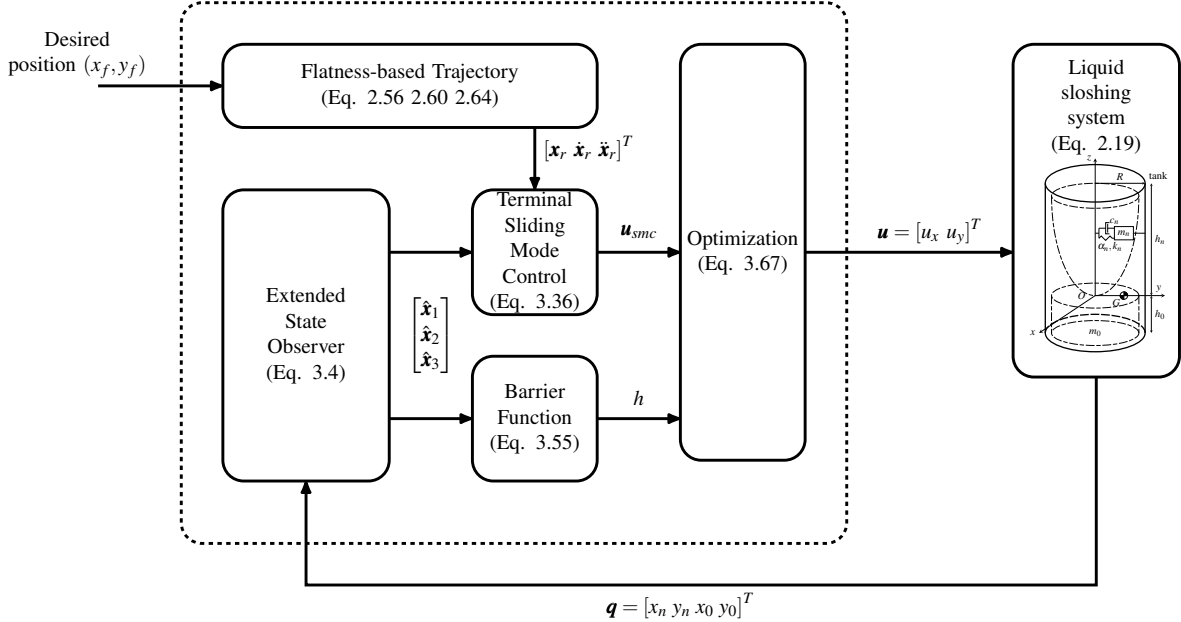


Figure 3.2: Second control architecture for liquid sloshing in a container

3.1 Extended State Observer

In practical terms, it is impossible to measure some state variables such as \dot{x}_n and \dot{y}_n . Also, the system is greatly affected by an unexpected disturbance. In order to estimate $\dot{\mathbf{q}}$ and disturbances, this research will propose an Extended State Observer. In the designed observer, if we denote $\mathbf{q}_1 = \mathbf{q}$ and $\mathbf{q}_2 = \dot{\mathbf{q}}$, and \mathbf{D} imply the disturbance component, then the state variables in the designed observer are defined as follows:

$$\begin{cases} \dot{\mathbf{q}}_1 = \mathbf{q}_2 \\ \dot{\mathbf{q}}_2 = \mathbf{M}^{-1} \mathbf{J} \mathbf{u} - \mathbf{M}^{-1} (\mathbf{G} + \mathbf{C} \dot{\mathbf{q}} + \mathbf{D}) \end{cases} \quad (3.1)$$

set $\mathbf{f}_q = -\mathbf{M}^{-1} (\mathbf{G} + \mathbf{C} \dot{\mathbf{q}})$ denotes the system's nonlinear parts and $\mathbf{d}_q = -\mathbf{M}^{-1} \mathbf{D}$ denotes the nonlinear function disturbances. We denote $\mathbf{M}_J = \mathbf{M}^{-1} \mathbf{J}$, then $\mathbf{u}_q = \mathbf{M}_J \mathbf{u}$. The state equation is rewritten as follows:

$$\begin{cases} \dot{\mathbf{q}}_1 = \mathbf{q}_2 \\ \dot{\mathbf{q}}_2 = \mathbf{q}_3 + \mathbf{u}_q \\ \dot{\mathbf{q}}_3 = \boldsymbol{\rho}(t) \end{cases} \quad (3.2)$$

where $\mathbf{q}_3 = \mathbf{f}_q + \mathbf{d}_q$ is the auxiliary variable and $\boldsymbol{\rho}(t)$ is the derivative of the function \mathbf{q}_3 . The state variable $\hat{\mathbf{x}}_i$ is defined as the observation of the state variable \mathbf{q}_i . Based on the generalized Extended State Observer (ESO) in [33, 34] a nonlinear ESO (NESO) will be designed to derive the immeasurable states and the lumped disturbances/uncertainties term. The state equation of the sloshing liquid container

is designed based on selected nonlinear function g_i as follows:

$$\begin{aligned}\dot{\hat{\mathbf{q}}}_1 &= \hat{\mathbf{q}}_2 + \delta^1 g_1 \left(\frac{\mathbf{q}_1 - \hat{\mathbf{q}}_1}{\delta^2} \right) \\ \dot{\hat{\mathbf{q}}}_2 &= \hat{\mathbf{q}}_3 + \delta^0 g_2 \left(\frac{\mathbf{q}_1 - \hat{\mathbf{q}}_1}{\delta^2} \right) + \mathbf{u}_q \\ \dot{\hat{\mathbf{q}}}_3 &= \delta^{-1} g_3 \left(\frac{\mathbf{q}_1 - \hat{\mathbf{q}}_1}{\delta^2} \right)\end{aligned}\quad (3.3)$$

If we chose the function $g_i(\cdot) = \sigma_i \times (\cdot)$ as the linear function, then the NESO becomes the linear ESO (LESO).

$$\begin{aligned}\dot{\hat{\mathbf{q}}}_1 &= \hat{\mathbf{q}}_2 + \frac{\sigma_1}{\delta} (\mathbf{q}_1 - \hat{\mathbf{q}}_1) \\ \dot{\hat{\mathbf{q}}}_2 &= \hat{\mathbf{q}}_3 + \frac{\sigma_2}{\delta^2} (\mathbf{q}_1 - \hat{\mathbf{q}}_1) + \mathbf{u}_q \\ \dot{\hat{\mathbf{q}}}_3 &= \frac{\sigma_3}{\delta^3} (\mathbf{q}_1 - \hat{\mathbf{q}}_1)\end{aligned}\quad (3.4)$$

Remark 6. Due to \mathbf{f}_q , $\frac{\partial \mathbf{f}_q}{\partial t}$, $\frac{\partial \mathbf{f}_q}{\partial \mathbf{q}_1}$, $\frac{\partial \mathbf{f}_q}{\partial \mathbf{q}_1}$ are vectors, matrices containing system parameters, position, velocity, and acceleration of the sloshing system. The parameters, position, velocity, and acceleration of the actuators are bounded. Therefore, there exist positive numbers p_{max} , v_{max} , a_{max} , c_1 , c_2 and c_3 such that $\|\mathbf{q}_1\| \leq p_{max}$, $\|\mathbf{q}_2\| \leq v_{max}$, $\|\dot{\mathbf{x}}_2\| \leq a_{max}$, $\|\frac{\partial \mathbf{f}_q}{\partial t}\| \leq p_m$, $\|\frac{\partial \mathbf{f}_q}{\partial \mathbf{q}_1}\| \leq c_1$, $\|\frac{\partial \mathbf{f}_q}{\partial \mathbf{q}_2}\| \leq c_2$, $\|\mathbf{u}_q\| \leq u_{max}$.

Assumption 1. The disturbance \mathbf{d}_q is continuous and differentiable with respect to their variables. Therefore, disturbance \mathbf{d}_q and its derivatives $\dot{\mathbf{d}}_x$ are bounded, which means $\|\mathbf{d}_q\| \leq d_{1c}$, $\|\dot{\mathbf{d}}_x\| \leq d_{2c}$, where d_{1c} and d_{2c} are positive constants.

Define the estimated errors as below:

$$\tilde{\mathbf{q}}_i(t) = (\mathbf{q}_i - \hat{\mathbf{q}}_i) / \delta^{4-i} \quad \forall i = 1, 2, 3 \text{ and } \tilde{\mathbf{q}} = [\tilde{\mathbf{q}}_1 \ \tilde{\mathbf{q}}_2 \ \tilde{\mathbf{q}}_3]^T \quad (3.5)$$

This definition leads to

$$\delta \dot{\tilde{\mathbf{q}}} = \mathbf{A} \tilde{\mathbf{q}} + \delta \mathbf{B} \boldsymbol{\rho} \quad (3.6)$$

where $\mathbf{A} = \begin{bmatrix} -\sigma_1 \mathbf{I}_4 & \mathbf{I}_4 & \mathbf{0}_4 \\ -\sigma_2 \mathbf{I}_4 & \mathbf{0}_4 & \mathbf{I}_4 \\ -\sigma_3 \mathbf{I}_4 & \mathbf{0}_4 & \mathbf{0}_4 \end{bmatrix}$ and $\mathbf{B} = \begin{bmatrix} \mathbf{0}_4 \\ \mathbf{0}_4 \\ \mathbf{I}_4 \end{bmatrix}$. Denote \mathbf{P} as a positive symmetrically defined matrix.

Theorem 3. Considering the sloshing model in (Eq. 2.19) and LESO in (Eq. 3.4). Under the view of Remark 6 and Assumption 1, if the constant number σ_1 , σ_2 , σ_3 are chosen such as

$$\mathbf{A} = \begin{bmatrix} -\sigma_1 \mathbf{I}_4 & \mathbf{I}_4 & \mathbf{0}_4 \\ -\sigma_2 \mathbf{I}_4 & \mathbf{0}_4 & \mathbf{I}_4 \\ -\sigma_3 \mathbf{I}_4 & \mathbf{0}_4 & \mathbf{0}_4 \end{bmatrix} \text{ is Hurwitz} \quad (3.7)$$

and we choose the positive δ small enough, then the estimation states will converge to the real states when $t \rightarrow \infty$, which means

$$\lim_{\delta \rightarrow 0} \left(\lim_{t \rightarrow \infty} \|\mathbf{q}_i - \hat{\mathbf{q}}_i\| \right) = 0 \quad \forall i = 1, 2, 3 \quad (3.8)$$

PROOF. The term $\boldsymbol{\rho}$ could be calculated as follow:

$$\begin{aligned} \boldsymbol{\rho}(t) &= \frac{d}{ds} \mathbf{f}_q(s, \mathbf{q}_1, \mathbf{q}_2) |_{s=\delta t} + \dot{\mathbf{d}}_x(s) \\ &= \frac{d}{d(\delta t)} \mathbf{f}_q(\delta t, \mathbf{q}_1, \mathbf{q}_2) + \dot{\mathbf{d}}_x(\delta t) \\ &= \frac{\partial}{\partial t} \mathbf{f}_q(\delta t, \mathbf{q}_1(\delta t), \mathbf{q}_2(\delta t)) + \frac{\partial}{\partial \mathbf{q}_1} \mathbf{f}_q(\delta t, \mathbf{q}_1(\delta t), \mathbf{q}_2(\delta t)) \mathbf{x}_2(\delta t) \\ &\quad + \frac{\partial}{\partial \mathbf{q}_2} \mathbf{f}_q(\delta t, \mathbf{q}_1(\delta t), \mathbf{q}_2(\delta t)) \mathbf{x}_3(\delta t) + \frac{\partial}{\partial \mathbf{q}_2} \mathbf{f}_q(\delta t, \mathbf{q}_1(\delta t), \mathbf{q}_2(\delta t)) \mathbf{u}_q + \dot{\mathbf{d}}_x(\delta t) \end{aligned} \quad (3.9)$$

Accompany to the Remark 6 and Assumption 1, there is exists of positive constant ρ_m satisfy:

$$\|\boldsymbol{\rho}(t)\| \leq \rho_m \quad (3.10)$$

Then the candidate Lyapunov function is selected as below:

$$V_{eso} = \delta \tilde{\mathbf{q}}^T \mathbf{P} \tilde{\mathbf{q}} \quad (3.11)$$

Taking the first derivative of candidate Lyapunov function V_{eso}

$$\begin{aligned} \frac{d}{dt} V_{eso} &= \delta \tilde{\mathbf{q}}^T \mathbf{P} \tilde{\mathbf{q}} + \delta \tilde{\mathbf{q}}^T \mathbf{P} \dot{\tilde{\mathbf{q}}} \\ &= (\mathbf{A} \tilde{\mathbf{q}} + \delta \mathbf{B} \boldsymbol{\rho})^T \mathbf{P} \tilde{\mathbf{q}} + \tilde{\mathbf{q}}^T \mathbf{P} (\mathbf{A} \tilde{\mathbf{q}} + \delta \mathbf{B} \boldsymbol{\rho}) \\ &= \tilde{\mathbf{q}}^T \mathbf{A}^T \mathbf{P} \tilde{\mathbf{q}} + \delta (\mathbf{B} \boldsymbol{\rho})^T \mathbf{P} \tilde{\mathbf{q}} + \tilde{\mathbf{q}}^T \mathbf{P} \mathbf{A} \tilde{\mathbf{q}} + \delta \mathbf{P} \mathbf{B} \boldsymbol{\rho} \end{aligned} \quad (3.12)$$

Since \mathbf{A} is Hurwitz, there existst an arbitrary positive symmetrically matrix \mathbf{Q} such that the following algebraic equations are satisfied:

$$\mathbf{A}^T \mathbf{P} + \mathbf{P} \mathbf{A} + \mathbf{Q} = 0 \quad (3.13)$$

Thus,

$$\begin{aligned} \frac{d}{dt} V_{eso} &= -\tilde{\mathbf{q}}^T \mathbf{Q} \tilde{\mathbf{q}} + 2\varepsilon \tilde{\mathbf{q}}^T \mathbf{P} \mathbf{B} \boldsymbol{\delta} \\ &\leq -\|\tilde{\mathbf{q}}\|^2 \lambda_{min}(\mathbf{Q}) + 2\varepsilon \|\tilde{\mathbf{q}}\| \|\mathbf{P} \mathbf{B}\| \rho_m \\ &\leq -V_{eso} \frac{\lambda_{min}(\mathbf{Q})}{\varepsilon \lambda_{max}(\mathbf{P})} + 2\varepsilon \sqrt{\frac{V_{eso}}{\varepsilon \lambda_{min}(\mathbf{P})}} \|\mathbf{P} \mathbf{B}\| \rho_m \end{aligned} \quad (3.14)$$

with $\lambda_{min}(\mathbf{Q})$ and $\lambda_{max}(\mathbf{P})$ are the minimum and the maximum eigenvalue of matrix \mathbf{Q} and matrix \mathbf{P} . Denote $\lambda_1 = \varepsilon \lambda_{max}(\mathbf{P})$, $\lambda_2 = \lambda_{min}(\mathbf{Q})$, and $\lambda_4 = \lambda_{min}(\mathbf{P})$. Since $\dot{V}_{eso} = \dot{V}_{eso} / (2\sqrt{V_1})$ we get

$$\frac{d}{dt} \sqrt{V_{eso}} \leq \frac{-\lambda_2}{2\lambda_1} \sqrt{V_{eso}} + \frac{\sqrt{\lambda_4 \varepsilon}}{\lambda_4} \|\mathbf{P} \mathbf{B}\| \rho_m \quad (3.15)$$

This is a standard first-order linear differential inequality, then it is upper-bounded by the solution of the corresponding equality.

$$\sqrt{V_{eso}(t)} \leq \left(\sqrt{V_{eso}(0)} - \frac{2\lambda_1\sqrt{\lambda_4}\varepsilon}{\lambda_2\lambda_4} \|\mathbf{PB}\|\rho_m \cdot \right) e^{\frac{-\lambda_2}{2\lambda_1}t} + \frac{2\lambda_1\sqrt{\lambda_4}\varepsilon}{\lambda_2\lambda_4} \|\mathbf{PB}\|\rho_m \quad (3.16)$$

then because of $\|\tilde{\mathbf{q}}\| \leq \sqrt{\frac{V_{eso}}{\varepsilon\lambda_4}}$ thus,

$$\|\tilde{\mathbf{q}}\| \leq \frac{\sqrt{\varepsilon\lambda_4 V_{eso}(0)}}{\varepsilon\lambda_4} e^{\frac{-\lambda_2}{2\lambda_1}t} - \frac{2\lambda_1}{\lambda_2\lambda_4} \|\mathbf{PB}\|\rho_m e^{\frac{-\lambda_2}{2\lambda_1}t} + \frac{2\lambda_1}{\lambda_2\lambda_4} \|\mathbf{PB}\|\rho_m = \mathcal{E}(t) \quad (3.17)$$

From Eqs.(3.5)(3.17), we have:

$$\|\mathbf{x}_i - \hat{\mathbf{x}}_i\| \leq \varepsilon^{4-i} (\mathcal{E}(t)) \quad (3.18)$$

where $i = 1, 2, 3$. Therefore by selecting the positive $\varepsilon \ll 1$, the error of the estimated state is bounded and convergence to the neighborhood of zero

$$\lim_{\varepsilon \rightarrow 0} \left(\lim_{t \rightarrow \infty} \|\mathbf{x}_i - \hat{\mathbf{x}}_i\| \right) = 0 \quad (3.19)$$

This is the end of the proof.

3.2 Lyapunov-based Model Predictive Control

From Equation 3.4, the estimated states $\hat{\mathbf{q}}_1$, $\hat{\mathbf{q}}_2$, and $\hat{\mathbf{q}}_3$ obtained from the LESO are employed to compute the control input \mathbf{u} and stabilize the sloshing dynamics. The reference trajectories \mathbf{q}_{1r} , \mathbf{q}_{2r} , and \mathbf{q}_{3r} are generated using a flatness-based time-optimal planning method. Define the tracking error as $\hat{\mathbf{e}} = \hat{\mathbf{q}}_1 - \mathbf{q}_{1r}$, where \mathbf{q}_{1r} is the desired trajectory. Given that \mathbf{q}_1 denotes the measured states, the sliding surface can be formulated as:

$$s = \boldsymbol{\lambda} \hat{\mathbf{e}} + \dot{\hat{\mathbf{e}}} = \boldsymbol{\lambda} (\hat{\mathbf{q}}_1 - \mathbf{q}_{1r}) + (\hat{\mathbf{q}}_2 - \mathbf{q}_{2r}) \quad (3.20)$$

where $\boldsymbol{\lambda} = \text{diag}(\lambda_{1c}, \lambda_{2c}, \lambda_{3c}, \lambda_{4c})$ is designed positive definite diagonal matrix. Since the system is underactuation, we could get the pseudo-inverse matrix $\mathbf{M}_J^+ = (\mathbf{M}_J^T \mathbf{M}_J)^{-1} \mathbf{M}_J^T$ of \mathbf{M}_J . We choose the reaching control law as follows:

$$\mathbf{u}_{eq} = -\mathbf{M}_J^+ (\hat{\mathbf{x}}_3 + \boldsymbol{\lambda} (\hat{\mathbf{x}}_2 - \dot{\mathbf{x}}_{r1}) - \mathbf{x}_{3r}) \quad (3.21)$$

is the pseudo-inverse matrix of \mathbf{Q} . In order to avoid the chattering phenomenon of SMC, we design the switching control law as:

$$\mathbf{u}_{sw} = -\mathbf{M}_J^+ [\boldsymbol{\mu}_1 s + \boldsymbol{\mu}_2 \text{sgn}(s)] \quad (3.22)$$

with $\boldsymbol{\mu}_1$, $\boldsymbol{\mu}_2$ are also designed positive definite diagonal matrix. Hence, the final control signal vector can be obtained:

$$\mathbf{u}_{smc} = \mathbf{u}_{eq} + \mathbf{u}_{sw} \quad (3.23)$$

Theorem 4. Consider the liquid system given in (Eq. 2.19), the system states are observed by the LESO described (Eq. 3.4), under control signal \mathbf{u}_{smc} given in (Eq. 3.23), the proposed sliding surface in (Eq. 3.20) is asymptotically convergence to zero.

PROOF. Select the Lyapunov function as

$$V = \frac{1}{2} \mathbf{s}^T \mathbf{s} \quad (3.24)$$

Considering the derivative of sliding surface (Eq. 3.20), ones can obtain:

$$\begin{aligned} \dot{\mathbf{s}} &= \boldsymbol{\lambda} \dot{\mathbf{e}} + \ddot{\mathbf{e}} \\ &= \boldsymbol{\lambda} (\dot{\mathbf{q}}_1 - \mathbf{q}_{2r}) + \dot{\mathbf{q}}_2 - \mathbf{q}_{3r} \\ &= \boldsymbol{\lambda} (\hat{\mathbf{q}}_2 + \frac{\sigma_1}{\delta} (\mathbf{q}_1 - \hat{\mathbf{q}}_1) - \mathbf{q}_{2r}) + \left(\hat{\mathbf{q}}_3 + \frac{\sigma_2}{\delta^2} (\mathbf{q}_1 - \hat{\mathbf{q}}_1) + \mathbf{u}_q \right) - \mathbf{q}_{3r} \\ &= \boldsymbol{\lambda} (\hat{\mathbf{q}}_2 + \frac{\sigma_1}{\delta} (\mathbf{q}_1 - \hat{\mathbf{q}}_1) - \mathbf{q}_{2r}) + \left(\hat{\mathbf{q}}_3 + \frac{\sigma_2}{\delta^2} (\mathbf{q}_1 - \hat{\mathbf{q}}_1) + \mathbf{u}_q \right) - \mathbf{q}_{3r} \end{aligned} \quad (3.25)$$

Then the derivative of V is determined as follows

$$\begin{aligned} \dot{V} &= \mathbf{s}^T \dot{\mathbf{s}} \\ &= \mathbf{s}^T \left(\boldsymbol{\lambda} \frac{\sigma_1}{\delta} \tilde{\mathbf{q}}_1 + \boldsymbol{\lambda} (\hat{\mathbf{q}}_2 - \mathbf{q}_{2r}) + \frac{\sigma_2}{\delta^2} \tilde{\mathbf{q}}_1 + (\hat{\mathbf{q}}_3 + \mathbf{M}_J \mathbf{u}) - \mathbf{q}_{3r} \right) \\ &= \mathbf{s}^T \left(\boldsymbol{\lambda} \frac{\sigma_1}{\delta} \tilde{\mathbf{q}}_1 + \frac{\sigma_2}{\delta^2} \tilde{\mathbf{q}}_1 - \boldsymbol{\mu}_1 \mathbf{s} - \boldsymbol{\mu}_2 \text{sgn}(\mathbf{s}) \right) \end{aligned} \quad (3.26)$$

From Theorem 3 it is clear that $\lim_{\delta \rightarrow 0} (\lim_{t \rightarrow \infty} \|\tilde{\mathbf{q}}_1\|) = 0$, then its could be derived from Equation 3.26 that

$$\dot{V} \approx \mathbf{s}^T (-\boldsymbol{\mu}_1 \mathbf{s} - \boldsymbol{\mu}_2 \text{sgn}(\mathbf{s})) \leq -\lambda_{min}(\boldsymbol{\mu}_2) \|\mathbf{s}\| - \lambda_{min}(\boldsymbol{\mu}_1) \|\mathbf{s}\|^2 < 0 \quad (3.27)$$

then the sliding surface s convergence to zero

$$\lim_{t \rightarrow \infty} \|\mathbf{s}\| = 0 \quad (3.28)$$

Therefore the theorem is proven. It is important to ensure that the parameters of the ESO are selected to guarantee a convergence rate faster than that of the SMC, thereby providing accurate state estimation in a timely manner for effective control. The proposed general LMPC scheme is obtained by solving the following optimal control problem:

$$\begin{aligned} \mathbf{u}_{lmpc} &= \underset{\mathbf{u}}{\operatorname{argmin}} \int_{t_0}^{t_0+T} (\hat{\mathbf{e}}(t) \mathbf{Q} \hat{\mathbf{e}}^T(t) + \tilde{\mathbf{u}}^T(t) \mathbf{R} \tilde{\mathbf{u}}(t)) dt \quad \forall k \in [1, N] \subset \mathbb{N} \\ \text{subject to } \quad &\hat{\mathbf{q}}_2 = \hat{\mathbf{f}}_q + \mathbf{u}_q + \hat{\mathbf{d}} \\ &\|\hat{\mathbf{q}}(t)\| \leq \mathbf{q}_{\max} \\ &\|\mathbf{u}(t)\| \leq \mathbf{u}_{\max} \\ &\dot{V}(\hat{\mathbf{q}}(t), \mathbf{u}(t)) \leq \dot{V}(\hat{\mathbf{q}}(t), \mathbf{u}_{smc}(t)) \end{aligned} \quad (3.29)$$

We define the tracking error as $\hat{\mathbf{e}}(t) = \hat{\mathbf{x}}_1(t) - \mathbf{x}_{1r}(t)$ and the control deviation as $\tilde{\mathbf{u}}(t) = \mathbf{u}(t) - \mathbf{u}_r(t)$. The matrices \mathbf{Q} and \mathbf{R} are positive definite weighting matrices. The control objective is formulated as the minimization of the cost function J . Notably, the choice of weights in \mathbf{Q} and \mathbf{R} significantly influences the control performance; hence, selecting appropriate values is essential to ensure the system prioritizes accurate trajectory tracking. Notice that normally in other Nonlinear Model Predictive control, the cost for the control energy is normally $\mathbf{u}^T \mathbf{R} \mathbf{u}$. However, thank to the flatness-based trajectory, we could compute the feed-forward control signal $\mathbf{u}_r = \ddot{\mathbf{x}}_{0r}$. Because we already know the ideal input \mathbf{u}_r , the optimization problem becomes easier — the solver doesn't have to guess the nominal control from scratch, only find the correction $\tilde{\mathbf{u}}$. Thereby maximizing information and helping the optimal solver return the control signal \mathbf{u} faster. Therefore, by solving this problem above, the LMPC controller will provide the control signals for tracking the desired trajectory while ensuring the region of states for the sloshing model. Reconsider the Lyapunov candidate function in (Eq. 3.23):

$$V = \frac{1}{2} \mathbf{s}^T \mathbf{s} \quad (3.30)$$

Taking utilization from the last constraint of the LMPC optimal problem:

$$\begin{aligned} \dot{V}(\hat{\mathbf{q}}(t), \mathbf{u}(t)) &= \mathbf{s}^T \left(\boldsymbol{\lambda} \frac{\sigma_1}{\delta} \tilde{\mathbf{q}}_1 + \frac{\sigma_2}{\delta^2} \tilde{\mathbf{q}}_1 + \boldsymbol{\lambda} (\hat{\mathbf{q}}_2(t) - \mathbf{x}_{r2}) + (\mathbf{M}_J \mathbf{u} + \hat{\mathbf{q}}_3(t)) - \mathbf{q}_{3r} \right) \\ &\leq \dot{V}(\hat{\mathbf{q}}, \mathbf{u}_{smc}(\hat{\mathbf{q}}(t))) \leq 0 \end{aligned} \quad (3.31)$$

This inequality implies the stabilization of the system under the LMPC method.

3.3 Terminal Sliding Mode Control with output constraint

3.3.1 Terminal sliding mode control

Similarly, the TSMC controller is using the estimation state variables $\hat{\mathbf{q}}_1$, $\hat{\mathbf{q}}_2$, and $\hat{\mathbf{q}}_3$ from ESO in Equation 3.4 to calculate the control signal applying to the sloshing model. The proposed terminal sliding surface is

$$\mathbf{s} = \hat{\mathbf{q}}_2 - \mathbf{q}_{2r} + (\mathbf{k}_1 + \mathbf{k}_2)(\hat{\mathbf{q}}_1 - \mathbf{q}_{1r}) + \mathbf{k}_1 \mathbf{k}_2 \int_0^t (\hat{\mathbf{q}}_1 - \mathbf{q}_{1r}) d\tau \quad (3.32)$$

where the trajectory based on flatness yields the reference vector \mathbf{q}_r , and $\mathbf{k}_1, \mathbf{k}_2 \in \mathbb{R}^{4 \times 4}$ are positive definite matrix. Denoting $\mathbf{k}_s = \mathbf{k}_1 + \mathbf{k}_2$ and $\mathbf{k}_p = \mathbf{k}_1 \mathbf{k}_2$, the equation above (Eq. 3.32) could be rewritten with the tracking errors and observing errors as follows:

$$\mathbf{s} = -\tilde{\mathbf{q}}_2 - \mathbf{k}_s \tilde{\mathbf{q}}_1 - \mathbf{k}_p \int_0^t \tilde{\mathbf{q}}_1 d\tau + \dot{\mathbf{e}} + \mathbf{k}_s \mathbf{e} + \mathbf{k}_p \int_0^t \mathbf{e} d\tau \quad (3.33)$$

It can be clearly seen that $\tilde{\mathbf{q}}_2 = \mathbf{q}_2 - \hat{\mathbf{q}}_2$ represents the observing velocity error, and $\tilde{\mathbf{q}}_1 = \mathbf{q}_1 - \hat{\mathbf{q}}_1$ represents the observing displacement error of the liquid container and sloshing mass. The symbol $\mathbf{e} = \mathbf{q}_1 - \mathbf{q}_{1r}$ indicates the tracking error of the

reference trajectory of the liquid sloshing system. The derivative of the terminal sliding surface is as follows:

$$\dot{\mathbf{s}} = -\dot{\tilde{\mathbf{q}}}_2 - \mathbf{k}_s \dot{\tilde{\mathbf{q}}}_1 - \mathbf{k}_p \tilde{\mathbf{q}}_1 + \ddot{\mathbf{e}} + \mathbf{k}_s \dot{\mathbf{e}} + \mathbf{k}_p \mathbf{e} \quad (3.34)$$

with $\ddot{\mathbf{e}} = \dot{\mathbf{q}}_2 - \ddot{\mathbf{q}}_r$. According to (Eq. 3.2), we obtain $\ddot{\mathbf{e}} = \mathbf{M}_J \mathbf{u} + \mathbf{q}_3 - \mathbf{q}_{3r}$. Then the derivative of the sliding surface is

$$\dot{\mathbf{s}} = -\dot{\tilde{\mathbf{q}}}_2 - \mathbf{k}_s \dot{\tilde{\mathbf{q}}}_1 - \mathbf{k}_p \tilde{\mathbf{q}}_1 + \mathbf{M}_J \mathbf{u} + \mathbf{q}_3 - \ddot{\mathbf{q}}_r + \mathbf{k}_s \dot{\mathbf{e}} + \mathbf{k}_p \mathbf{e} \quad (3.35)$$

The control signal of Terminal Sliding Mode Control (TSMC) based ESO is proposed as follows:

$$\begin{aligned} \mathbf{u}_{tsmc} = & -\mathbf{M}_J^+ \left(\hat{\mathbf{q}}_3 + \mathbf{k}_s (\hat{\mathbf{q}}_2 - \mathbf{q}_{2r}) + \mathbf{k}_p (\hat{\mathbf{q}}_1 - \mathbf{q}_{1r}) \right. \\ & \left. - \mathbf{q}_{3r} + \boldsymbol{\lambda} \mathbf{s} + \boldsymbol{\mu}_1 \text{diag}(\text{sgn}(\mathbf{s})) |\mathbf{s}|^\alpha + \boldsymbol{\mu}_2 \text{sgn}(\mathbf{s}) \right) \end{aligned} \quad (3.36)$$

where $\boldsymbol{\mu}_1 = \text{diag}(\mu_{11}, \mu_{12}, \mu_{13}, \mu_{14})$, $\boldsymbol{\lambda} = \text{diag}(\lambda_{1c}, \lambda_{2c}, \lambda_{3c}, \lambda_{4c})$, $\boldsymbol{\mu}_2 = \text{diag}(\mu_{21}, \mu_{22}, \mu_{23}, \mu_{24})$ are positive definite designed matrices. The control parameter α must satisfy the condition $0 < \alpha < 1$. We want to emphasize that the term $\boldsymbol{\mu}_1 \text{diag}(\text{sgn}(\mathbf{s})) |\mathbf{s}|^\alpha$ accelerates the convergence speed in the TSMC algorithm.

Theorem 5. *Considering the liquid sloshing system (Eq. 2.19), the ESO (Eq. 3.4), the sliding surface (Eq. 3.33) and the control signal of Terminal Sliding Mode Control base ESO (Eq. 3.36). The estimated state variables $\hat{\mathbf{q}}_i$ will converge to the real state variables \mathbf{x}_i , the terminal sliding surface \mathbf{s} and the tracking error \mathbf{e} is asymptotically converged to zero. In other words, we have*

$$\begin{aligned} \lim_{t \rightarrow T_s} \hat{\mathbf{q}}_i &= \mathbf{q}_i \quad \forall i = 1, 2, 3 \\ \lim_{t \rightarrow T_s} \|\mathbf{s}\| &= 0 \\ \lim_{t \rightarrow T_s} \|\mathbf{e}\| &= 0 \end{aligned} \quad (3.37)$$

PROOF. Replacing the proposed TSMC (Eq. 3.36) in the derivative of the terminal sliding surface (Eq. 3.35), we obtain

$$\dot{\mathbf{s}} = \tilde{\mathbf{q}}_3 - \dot{\tilde{\mathbf{q}}}_2 - \boldsymbol{\lambda} \mathbf{s} - \boldsymbol{\mu}_1 \text{diag}(\text{sgn}(\mathbf{s})) |\mathbf{s}|^\alpha - \boldsymbol{\mu}_2 \text{sgn}(\mathbf{s}) \quad (3.38)$$

with $\tilde{\mathbf{q}}_3 = \mathbf{q}_3 - \hat{\mathbf{q}}_3$ representing the estimation error of total disturbance. The estimated error variable $\tilde{\mathbf{q}}_2$ is determined from (Eq. 3.3) and (Eq. 3.4)

$$\dot{\tilde{\mathbf{q}}}_2 = \tilde{\mathbf{q}}_3 - \frac{\alpha_2}{\varepsilon^2} \tilde{\mathbf{q}}_1 \quad (3.39)$$

Subsequently, the derivative of the terminal sliding surface could be described as

$$\dot{\mathbf{s}} = \frac{\alpha_2}{\varepsilon^2} \tilde{\mathbf{q}}_1 - \boldsymbol{\lambda} \mathbf{s} - \boldsymbol{\mu}_1 \text{diag}(\text{sgn}(\mathbf{s})) |\mathbf{s}|^\alpha - \boldsymbol{\mu}_2 \text{sgn}(\mathbf{s}) \quad (3.40)$$

The Lyapunov candidate is chosen as

$$V = \frac{1}{2} \mathbf{s}^T \mathbf{s} \quad (3.41)$$

Taking the derivative of the Lyapunov function, then replacing the (Eq. 3.40) in the equation, we have

$$\begin{aligned} \dot{V} &= \mathbf{s}^T \left(\frac{\alpha_2}{\varepsilon^2} \tilde{\mathbf{q}}_1 - \boldsymbol{\lambda} \mathbf{s} - \boldsymbol{\mu}_1 \text{diag}(\text{sgn}(\mathbf{s})) |\mathbf{s}|^\alpha - \boldsymbol{\mu}_2 \text{sgn}(\mathbf{s}) \right) \\ &= -\mathbf{s}^T \boldsymbol{\mu}_2 \text{sgn}(\mathbf{s}) - \mathbf{s}^T \boldsymbol{\lambda} \mathbf{s} - |\mathbf{s}^T| \boldsymbol{\mu}_1 |\mathbf{s}|^\alpha \\ &\quad + \frac{\alpha_2}{\varepsilon^2} \mathbf{s}^T \tilde{\mathbf{q}}_1 \end{aligned} \quad (3.42)$$

According to Theorem 3, because of

$$\begin{aligned} -\mathbf{s}^T \boldsymbol{\mu}_2 \text{sgn}(\mathbf{s}) &\leq 0 \\ \lim_{\delta \rightarrow 0} \frac{\alpha_2}{\delta^2} \mathbf{s}^T \tilde{\mathbf{q}}_1 &= 0 \end{aligned} \quad (3.43)$$

Thus, the equation (Eq. 3.42) is satisfied

$$\begin{aligned} \dot{V} &\leq -\|\mathbf{s}\|^2 (\lambda_{min}) - \mu_{1,min} \sum_{i=1}^4 |s_i|^{\alpha+1} \\ &= -\Lambda_1 V - \Lambda_2 V^\mu \end{aligned} \quad (3.44)$$

where $\lambda_{min} = \min(\lambda_{1c}, \lambda_{2c}, \lambda_{3c}, \lambda_{4c})$, $\mu_{min} = \min(\mu_{11}, \mu_{12}, \mu_{13}, \mu_{14})$, $\Lambda_1 = 2(\lambda_{min})$ and $\Lambda_2 = \mu_{min} 2^\mu$ with $\mu = \frac{\alpha+1}{2}$.

Lemma 6. According to [35], if the Lyapunov function is a continuous function that satisfies Eq. (3.45) then V converges to zero in the settling-time function T_f which is the upper boundary is determined as (3.46)

$$\dot{V}(t) \leq -a_1 V(t) - a_2 V^{a_3}(t) \quad \forall V(t_0) > 0, t > t_0 \quad (3.45)$$

and

$$T_f = t_0 + \frac{1}{a_1(1-a_3)} \ln \left(\frac{a_1 V^{1-a_3}(t_0) + a_2}{a_2} \right) \quad (3.46)$$

where $a_1, a_2 > 0$ and a_3 satisfies $0.5 < a_3 < 1$

Because of $0 < \alpha < 1$ then $0.5 < \mu < 1$. According to Lemma 6 and (Eq. 3.44) then $V(t)$ will converge to zero in a finite time with an upper boundary T_s .

$$T_s = t_0 + \frac{1}{\Lambda_1(1-\mu)} \ln \left(\frac{\Lambda_1 V^{1-\mu}(t_0) + \Lambda_2}{\Lambda_2} \right) \quad (3.47)$$

where t_0 is the initial time value. Then the terminal sliding surface \mathbf{s} converges to zero after a duration T_s . From (Eq. 3.33), the terminal sliding surface can also be written as

$$\mathbf{s} = -\mathbf{s}_o - \mathbf{k}_1 \int_0^t \mathbf{s}_o d\tau + \mathbf{s}_c + \mathbf{k}_1 \int_0^t \mathbf{s}_c d\tau \quad (3.48)$$

where $\mathbf{s}_o = \tilde{\mathbf{q}}_2 + \mathbf{k}_2 \tilde{\mathbf{x}}_1$ and $\mathbf{s}_c = \dot{\mathbf{e}} + \mathbf{k}_2 \mathbf{e}$. From Lemma 6, the Lyapunov function converges to zero after the finite time T_s then

$$\lim_{t \rightarrow T_s} \mathbf{s} = \lim_{t \rightarrow T_s} \left(-\mathbf{s}_o - \mathbf{k}_1 \int_0^t \mathbf{s}_o d\tau + \mathbf{s}_c + \mathbf{k}_1 \int_0^t \mathbf{s}_c d\tau \right) = 0 \quad (3.49)$$

In the previous section, according to (Theorem 3), the observing error $\tilde{\mathbf{x}}_i$ converges to zero, which means the

$$\lim_{\varepsilon \rightarrow 0} \left(\lim_{t \rightarrow \infty} \mathbf{s}_o \right) = \lim_{\varepsilon \rightarrow 0} \left(\lim_{t \rightarrow \infty} \tilde{\mathbf{q}}_2 + \mathbf{k}_2 \tilde{\mathbf{q}}_1 \right) = 0 \quad (3.50)$$

then we could easily obtain

$$\lim_{t \rightarrow T_s} \left\| \mathbf{s}_c + \mathbf{k}_1 \int_0^t \mathbf{s}_c d\tau \right\| = 0 \quad (3.51)$$

then the tracking error in a finite time T_s would satisfy

$$\begin{aligned} \lim_{t \rightarrow T_s} \|\dot{\mathbf{e}} + \mathbf{k}_2 \mathbf{e}\| &= 0 \\ \lim_{t \rightarrow T_s} \|\mathbf{e}\| &= \lim_{t \rightarrow T_s} \|\mathbf{e}^{-\mathbf{k}_2 t}\| = 0 \end{aligned} \quad (3.52)$$

This is the end of the proof.

3.3.2 Control Barrier Function

During this design phase, we propose a method to limit the maximum height of liquid sloshing within the system. The objective of ensuring safety can be explained as follows: given the container's capacity constraint, there is a risk of liquid spillage from the tank. First introduced [26, 36], CBF is an effective output constraint method, by considering a superlevel set of continuously differentiable $h : \chi \rightarrow \mathbb{R}$ ($\chi \subset \mathbb{R}^8$ is the set of \mathbf{x}) as below:

$$\begin{aligned} \mathcal{C} &= \{x \in \chi \subset \mathbb{R}^8 : h(x) \geq 0\} \\ \partial \mathcal{C} &= \{x \in \chi \subset \mathbb{R}^8 : h(x) = 0\} \\ \text{Int}(\mathcal{C}) &= \{x \in \chi \subset \mathbb{R}^8 : h(x) > 0\} \end{aligned} \quad (3.53)$$

Definition 3. A safe set \mathcal{C} is forward invariant of the system (Eq. 2.19) if the solutions with any initial condition $\mathbf{x}_0 \in \mathcal{C}$, $\mathbf{x}(t_0) \in \mathcal{C}$ for $\mathbf{x}(t_0) = \mathbf{x}_0$ and $t_0 \in I(\mathbf{x}_0) = [0, t_{max}]$. The system (2.19) is safe with respect to the set \mathcal{C} if the set \mathcal{C} is forward invariant.

Definition 4. Given a safe set $\mathcal{C} \subset \chi$, consider the system (Eq. 2.19), if there exists a class κ_∞ function $\alpha(\cdot)$, the function $h : \chi \rightarrow \mathbb{R}$ is a zeroing CBF (ZCBF) satisfying

$$\begin{aligned} \sup_{\mathbf{u} \in \mathcal{U}} (L_f h(\mathbf{x}) + L_g h(\mathbf{x}) \mathbf{u}) &\geq -\gamma(h(\mathbf{x})) \\ \frac{\partial h}{\partial \mathbf{x}} &\neq \mathbf{0}_{8 \times 1} \quad \forall \mathbf{x} \in \partial \mathcal{C} \end{aligned} \quad (3.54)$$

If $\gamma(h(\mathbf{x})) = \alpha_{cbf} h(\mathbf{x})$, then the function $h(\mathbf{x})$ is a ZCBF if and only if α_{cbf} is a positive real number.

Therefore, in this study, we establish a safe threshold for the liquid sloshing height with Quadratic Programming (QP) to ensure the effectiveness of the overall control algorithms. With $0 < c_\varepsilon \ll 1$, the constraint function h is given as follows:

$$h(\mathbf{x}) = \bar{\eta}_{max}^2 - \left(\frac{\xi_{11}^2 h m_1}{m_F R} \right)^2 (x_1^2 + y_1^2) - c_\varepsilon (\dot{x}_1^2 + \dot{y}_1^2) \geq 0 \quad (3.55)$$

where $\mathbf{x} = [\mathbf{q}^T \quad \dot{\mathbf{q}}^T]^T$.

Remark 7. If the barrier certificate h is chosen only depending on the output of the system, then the constraint in QP shows that the input \mathbf{u} only influences the system for $L_g h(\mathbf{x}) \neq 0$. Therefore, by adding a very small coefficient of the first output's derivative $\dot{\mathbf{x}}$ in the barrier certificate $h(\mathbf{x})$ [37], then $h(\mathbf{x})$ depends directly on \mathbf{u} . If the term $\dot{\mathbf{x}}$ is neglected, the CBF will have a relative degree greater than one and will be discussed in our future work.

Denote $\mathbf{f} = \mathbf{M}^{-1}(-\mathbf{C}\dot{\mathbf{q}} - \mathbf{G} - \mathbf{D})$ and $\mathbf{g} = \mathbf{M}_J$, the system in (Eq. 2.19) could be rewritten as:

$$\dot{\mathbf{x}} = \mathcal{A}\mathbf{x} + \mathcal{B}(\mathbf{f} + \mathbf{g}\mathbf{u}) \quad (3.56)$$

where $\mathcal{A} = \begin{bmatrix} \mathbf{0}_{4 \times 4} & \mathbf{I}_{4 \times 4} \\ \mathbf{0}_{4 \times 4} & \mathbf{0}_{4 \times 4} \end{bmatrix}$, and $\mathcal{B} = \begin{bmatrix} \mathbf{0}_{4 \times 4} \\ \mathbf{I}_{4 \times 4} \end{bmatrix}$ then a safe set \mathcal{C} is defined as a super-level set of $h(\mathbf{x})$

$$\mathcal{C} = \{\mathbf{x} \in \chi \subset \mathbb{R}^8 : h(\mathbf{x}) \geq 0\} \quad (3.57)$$

However, to compensate for the uncertainty disturbances, the ESO-based CBF is introduced by giving a candidate Zeroing CBF [38], which includes the uncertainty term as

$$H(\mathbf{x}, \hat{\mathbf{f}}) = h(\mathbf{x}) - \varepsilon \hat{\mathbf{e}}^T \mathbf{P} \hat{\mathbf{e}} \quad (3.58)$$

Theorem 7. Take into consideration the superlevel set C of a differentiable continuously $h(x)$ and the liquid system given in equation (2.39), as well as the ESO given in equation (2.46) $h(\mathbf{x}) : \rightarrow \mathbb{R}$ as described in (2.80), if the derivative of the extended state $\|\dot{\mathbf{f}}_x\| \leq \rho_m$ is bounded, if the chosen matrix \mathbf{Q} is satisfied $\lambda_2 \geq \alpha_{cbf} \lambda_3$ where $\lambda_3 = \varepsilon \lambda_1$, and the initial condition of $h(\mathbf{x}(0)) \geq \varepsilon \lambda_1$, then the set \mathcal{C} is called the safe set with the control signal \mathbf{u} satisfy:

$$\begin{aligned} \mathbf{u} \in \mathcal{K}_h = \left\{ \mathbf{v} \in \mathcal{U} \mid L_f h(\mathbf{x}) + L_g h(\mathbf{x}) \mathbf{v} - \left\| \frac{\partial h}{\partial \mathbf{x}} \right\| \mathcal{E}(t) \right. \\ \left. - \frac{1}{4} \left(1 + \frac{1}{\lambda_2 - \alpha_{cbf} \lambda_3} \left\| \frac{\partial h}{\partial \mathbf{x}} \right\|^2 \right) - 2\mathcal{E}(t)^2 - \varepsilon^2 \rho_m^2 \|\mathbf{P} \mathbf{B}\|^2 + \alpha_{cbf} h(\mathbf{x}) \geq 0 \right\} \quad (3.59) \end{aligned}$$

PROOF. Defining the time derivatives of the ZCBF \dot{H} as follows:

$$\dot{H}(\mathbf{x}) = \frac{\partial h}{\partial \mathbf{x}} (\mathbf{g}\mathbf{u} + \mathbf{f}) + \frac{\partial h}{\partial t} - 2\varepsilon \hat{\mathbf{e}}^T \mathbf{P} \dot{\hat{\mathbf{e}}} \quad (3.60)$$

$$\geq \frac{\partial h}{\partial \mathbf{x}}^T (\mathbf{g}\mathbf{u} + \hat{\mathbf{f}}) + \frac{\partial h}{\partial \mathbf{x}}^T e_3 + \frac{\partial h}{\partial t} + \|\hat{\mathbf{e}}\|^2 \lambda_{min}(\mathbf{Q}) - 2\varepsilon \|\hat{\mathbf{e}}\| \cdot \|\mathbf{P} \mathbf{B}\| \rho_m \quad (3.61)$$

According to Cauchy's inequality, yields

$$\begin{aligned} \dot{H} &\geq \frac{\partial h^T}{\partial \mathbf{x}} (\mathbf{g}\mathbf{u} + \hat{\mathbf{f}}) + \frac{\partial h^T}{\partial \mathbf{x}} \hat{e}_3 + \frac{\partial h}{\partial t} + \|\hat{\mathbf{e}}\|^2 (\lambda_2 - \alpha\lambda_3) + \alpha\lambda_3 \|\hat{\mathbf{e}}\|^2 - \|\hat{\mathbf{e}}\|^2 - (\varepsilon \|\mathbf{PB}\| \rho_m) \\ &\quad (3.62) \end{aligned}$$

$$\begin{aligned} &\geq \frac{\partial h^T}{\partial \mathbf{x}} (\mathbf{g}\mathbf{u} + \hat{\mathbf{f}}) + \left\| \frac{1}{2} \frac{\partial h^T}{\partial \mathbf{x}} + \hat{e}_3 \right\|^2 - \left\| \frac{1}{2} \frac{\partial h}{\partial \mathbf{x}} \right\|^2 - \|\hat{e}_3\|^2 - \|\hat{\mathbf{e}}\|^2 - \frac{1}{4(\lambda_2 - \alpha\lambda_3)} \left\| \frac{\partial h}{\partial \mathbf{x}} \right\|^2 \\ &\quad (3.63) \end{aligned}$$

$$\begin{aligned} &+ \frac{\partial h}{\partial t} - \frac{\partial h^T}{\partial \mathbf{x}} \|\hat{\mathbf{e}}\| + \left\| \sqrt{\lambda_2 - \alpha\lambda_3} \|\hat{\mathbf{e}}\| + \frac{1}{2\sqrt{\lambda_2 - \alpha\lambda_3}} \frac{\partial h^T}{\partial \mathbf{x}} \right\|^2 - (\varepsilon \|\mathbf{PB}\| \rho_m)^2 + \alpha\lambda_3 \|\hat{\mathbf{e}}\|^2 \\ &\quad (3.64) \end{aligned}$$

According to (Eq. 3.59) $\mathbf{u} \in \mathcal{K}_h$, thus

$$\begin{aligned} \dot{H}(\mathbf{x}) &\geq \left\| \frac{\partial h}{\partial \mathbf{x}} \right\| \mathcal{E}(t) + \frac{1}{4} \left(1 + \frac{1}{\lambda_2 - \alpha\lambda_3} \right) \left\| \frac{\partial h}{\partial \mathbf{x}} \right\|^2 + \mathcal{E}(t)^2 + (\varepsilon \|\mathbf{PB}\| \rho_m)^2 - \alpha h \\ &+ \left\| \frac{1}{2} \frac{\partial h^T}{\partial \mathbf{x}} + \hat{e}_3 \right\|^2 - \left\| \frac{1}{2} \frac{\partial h}{\partial \mathbf{x}} \right\|^2 - \|\hat{e}_3\|^2 - \|\hat{\mathbf{e}}\|^2 - \frac{1}{4(\lambda_2 - \alpha\lambda_3)} \left\| \frac{\partial h}{\partial \mathbf{x}} \right\|^2 + \frac{\partial h}{\partial t} \\ &- \frac{\partial h^T}{\partial \mathbf{x}} \|\hat{\mathbf{e}}\| + \left\| \sqrt{\lambda_2 - \alpha\lambda_3} \|\hat{\mathbf{e}}\| + \frac{1}{2\sqrt{\lambda_2 - \alpha\lambda_3}} \frac{\partial h^T}{\partial \mathbf{x}} \right\|^2 - (\varepsilon \|\mathbf{PB}\| \rho_m)^2 + \alpha\lambda_3 \|\hat{\mathbf{e}}\|^2 \\ &\quad (3.65) \end{aligned}$$

Simplify the above equation, we obtain

$$\begin{aligned} \dot{H}(\mathbf{x}) &\geq \left\| \frac{\partial h}{\partial \mathbf{x}} \right\| \mathcal{E}(t) + 2\mathcal{E}(t)^2 - \|\hat{e}_3\|^2 - \|\hat{\mathbf{e}}\|^2 + \alpha\lambda_3 \|\hat{\mathbf{e}}\|^2 - \alpha h \\ &\geq -\alpha H(\mathbf{x}) \quad (3.66) \end{aligned}$$

Then, with an initial condition of $H(\mathbf{x}(0)) > 0$, we get $H(\mathbf{x}) \geq 0 \forall t$. As a result, we have $h \geq V_{ESO} \geq 0$. Hence, the set \mathcal{C} is forward invariant. This is the end of the proof.

Finally, to achieve the constraint in sloshing height based on the nominal TSMC controller, the problem could be written in quadratic form as follows:

$$\begin{aligned} \mathbf{u} = \underset{\mathbf{v}}{\operatorname{argmin}} \|\mathbf{v} - \mathbf{u}_{tsmc}\|^2 &= \mathbf{v}^T \mathbf{v} - 2\mathbf{u}_{tsmc}^T \mathbf{v} + \mathbf{u}_{tsmc}^T \mathbf{u}_{tsmc} \\ \text{subject to } L_g h \mathbf{v} + L_f h - \left\| \frac{\partial h}{\partial \mathbf{x}} \right\| \mathcal{E}(t) - \frac{1}{4} \left(1 + \frac{1}{\lambda_2 - \alpha\lambda_3} \right) \left\| \frac{\partial h}{\partial \mathbf{x}} \right\|^2 &\quad (3.67) \\ - 2\mathcal{E}(t)^2 - \varepsilon^2 \rho_m^2 \|\mathbf{PB}\|^2 + \alpha h &\geq 0 \end{aligned}$$

The optimization could be solved by quadratic programming. We also can express the control input as the explicit solution to satisfy the safety constraint ZCBF $h(\mathbf{x})$.

Denote the control u_{cbf} as follow:

$$\mathbf{u}_{cbf} = \begin{cases} -\frac{I_h(\mathbf{x}, \mathbf{u}_{tsmc}) - J_h(\mathbf{x})}{\|L_g h(\mathbf{x})\|^2} (L_g h(\mathbf{x}))^T & , \quad I_h(\mathbf{x}, \mathbf{u}_{tsmc}) < J_h(\mathbf{x}) \\ \mathbf{0}_{2 \times 1} & , \quad I_h(\mathbf{x}, \mathbf{u}_{tsmc}) \geq J_h(\mathbf{x}) \end{cases} \quad (3.68)$$

where

$$\begin{aligned} I_h(\mathbf{x}, \mathbf{u}_{hsmc}) &= L_f h(\mathbf{x}) + L_g h(\mathbf{x}) \mathbf{u}_{hsmc} \\ J_h(\mathbf{x}) &= \left\| \frac{\partial h}{\partial \mathbf{x}} \right\| \mathcal{E}(t) + \frac{1}{4} \left(1 + \frac{1}{\lambda_2 - \alpha \lambda_3} \left\| \frac{\partial h}{\partial \mathbf{x}} \right\|^2 \right) + 2\mathcal{E}(t)^2 + \varepsilon^2 \rho_m^2 \|\mathbf{PB}\|^2 - \alpha h(\mathbf{x}) \end{aligned} \quad (3.69)$$

Then the final control signals \mathbf{u} is

$$\mathbf{u} = \mathbf{u}_{tsmc} + \mathbf{u}_{cbf} \quad (3.70)$$

CHAPTER 4: NUMERICAL SIMULATIONS

In this chapter, we carry out some simulations with a cylindrical container and the chosen liquid is water with the distinctive dynamic viscosity ν and density ρ , respectively. The model parameters are given in the below table.

Table 4.1: Parameters of the liquid sloshing system

Model Parameter	Value	Unit	Designed Parameter	Value	Unit
R	50	mm	x_i	0	m
h	70	mm	x_f	4	m
g	9.81	m/s^2	y_i	0	m
ρ	997	kg/m	y_f	3	m
ν	10^{-6}	m^2/s	t_f (optimized solution)	6.0901	s
α	0.58	-	$\mathbf{u}_{0(max)}$	0.5	m/s^2
w	2	-	$\bar{\eta}_{n(max)}$	2.5	mm
ξ_{11}	1.841	-	N	200	-
ω_1	18.8968	rad/s	-	-	-
ζ_1	0.0042	-	-	-	-

The parameters of the Extended State Observer (ESO), as elaborated in Section 3.1, play crucial roles in achieving effective disturbance rejection. The immeasurable state variables $\dot{\mathbf{q}}$, which are required for all of the above controllers, are estimated from the LESO. In this study, we choose the parameter as $\alpha_1 = 50$, $\alpha_2 = 50$, $\alpha_3 = 100$, and $\varepsilon = 0.0005$. For the LMPC controller has weighted matrices $\mathbf{Q}_{mpc} = \text{diag} [1000 \ 1000 \ 100 \ 100 \ 5 \ 5 \ 5]$ and $\mathbf{R}_{mpc} = \text{diag} [0.1 \ 0.1]$ are positive weighted matrices. And for the Terminal Sliding Mode Control (TSMC) controller, these control parameters are given as below:

$$\begin{aligned} \mathbf{k}_s &= \text{diag} [2.625 \ 2.625 \ 0.5 \ 0.5] & \boldsymbol{\mu}_1 &= \text{diag} [4.2 \ 4.2 \ 0.8 \ 0.8] \\ \mathbf{k}_p &= \text{diag} [0.7875 \ 0.7875 \ 0.7875 \ 0.7875] & \boldsymbol{\mu}_2 &= \text{diag} [0.015 \ 0.015 \ 0.3 \ 0.3] \\ \boldsymbol{\lambda} &= \text{diag} [1.575 \ 1.575 \ 0.3 \ 0.3] & \alpha &= 0.3 \end{aligned}$$

To proof the effectiveness of the proposed control algorithm, we will use a classical Sliding Mode Control (SMC) with control law in Equation 3.23 and Linear-quadratic regulator (LQR) controller to compare with the proposed controllers. The parameters of SMC are chosen as $\boldsymbol{\lambda}_{smc} = [1.1 \ 1.1 \ 0.2 \ 0.2]$, $\boldsymbol{\mu}_{1smc} = [2.75 \ 2.75 \ 0.5 \ 0.5]$ and $\boldsymbol{\mu}_{2smc} = [1.5 \ 1.5 \ 0.5 \ 0.5]$. The LQR controller is designed by the linearization system in Equation 2.19:

$$\dot{\mathbf{x}} = \mathbf{A}_{linear} \mathbf{x} + \mathbf{B}_{linear} \mathbf{u} \quad (4.1)$$

where $\mathbf{x} = \begin{bmatrix} \mathbf{q} & \dot{\mathbf{q}} \end{bmatrix}$ and

$$\mathbf{A}_{linear} = \begin{bmatrix} 0 & 0 & 0 & 0 & 1 & 0 & 0 & 0 \\ 0 & 0 & 0 & 0 & 0 & 1 & 0 & 0 \\ 0 & 0 & 0 & 0 & 0 & 0 & 1 & 0 \\ 0 & 0 & 0 & 0 & 0 & 0 & 0 & 1 \\ -\omega_1^2 & 0 & 0 & 0 & -2\omega_1\zeta_1 & 0 & 0 & 0 \\ 0 & -\omega_1^2 & 0 & 0 & 0 & -2\omega_1\zeta_1 & 0 & 0 \\ 0 & 0 & 0 & 0 & 0 & 0 & 0 & 0 \\ 0 & 0 & 0 & 0 & 0 & 0 & 0 & 0 \end{bmatrix} \quad \mathbf{B}_{linear} = \begin{bmatrix} 0 & 0 \\ 0 & 0 \\ 0 & 0 \\ 0 & 0 \\ -1 & 0 \\ 0 & -1 \\ 1 & 0 \\ 0 & 1 \end{bmatrix} \quad (4.2)$$

Selecting the matrices $\mathbf{Q}_{LQR} = \text{diag} [1000 \ 1000 \ 100 \ 100 \ 5 \ 5 \ 5 \ 5]$ and $R_{LQR} = 0.01$, the controller can be found

$$\mathbf{K}_{LQR} = \begin{bmatrix} -31.1 & 0 & -9.8 & 0 & 2.2 & 0 & 3.1 & 0 \\ 0 & -31.1 & 0 & -9.8 & 0 & 2.2 & 0 & 3.1 \end{bmatrix} \quad (4.3)$$

And to compensate for the lumped disturbance, the LQR control signal is $\mathbf{u} = -\mathbf{K}[\hat{\mathbf{x}}_1 \ \hat{\mathbf{x}}_2]^T - \mathbf{B}^{-1}\mathbf{D}$. I want to emphasize that those above parameters would be used in every following simulation scenarios. The goal of the simulations is to validate the following points:

- **Effectiveness of Trajectory Planning:** Do the proposed trajectory planning methods perform effectively? How do they compare to existing motion planning approaches in terms of performance and efficiency?
- **Controller Performance:** Is the proposed controller capable of accurately tracking the desired trajectory, even in the presence of external disturbances?
- **Sloshing Constraint Satisfaction:** Does the system successfully maintain the sloshing height below the predefined maximum threshold, ensuring constraint satisfaction during motion?

To answer these questions, subsequently, I will introduce three simulation scenarios including:

- **First Scenario:** Since most of the traditional anti-sloshing methods just worked for the straight line. Therefore, to be fair, we will compare the performance of different trajectory planning methods given the same amount of transferring time and distance.
- **Second Scenario:** To efficiently navigate through this environment and minimize traversal time, a flatness-based time-optimal trajectory planning strategy is employed. This approach enables the container to dynamically avoid obstacles while maintaining high-speed and efficient motion along the trajectory.

- **Third Scenario:** This scenario builds upon the second by introducing white noise into the acceleration input and there is a small changes in model dynamics $\ddot{\mathbf{q}}_{practical}$ (given as below), simulating real-world disturbances and uncertainties. Here, the effectiveness of the Extended State Observer (ESO) is demonstrated, as it estimates the disturbances in real-time and enables the controller to compensate accordingly. This showcases the ESO's capability in enhancing system robustness under uncertain conditions.

$$\ddot{\mathbf{q}}_{practical} = (1 + 0.1 \sin(50t)) \ddot{\mathbf{q}}_{no} \quad (4.4)$$

4.1 Comparing different motion planning approaches

In this scenario, the container is tasked with traversing from its initial position at coordinates $(0, 0)$ to a designated endpoint located at $(8, 6)$. We compare 4 different motion planning which are basic 212 motions (212), input shaping (IS) approach, rest-to-rest trajectory (R2R), and time-optimize flatness-based approach to moving the container from $(0, 0)$ to $(8, 6)$. The transfer time $T = 3.5\text{s}$, and the total distance is 10m. The (Fig. 4.1) gives us the position of the liquid con-

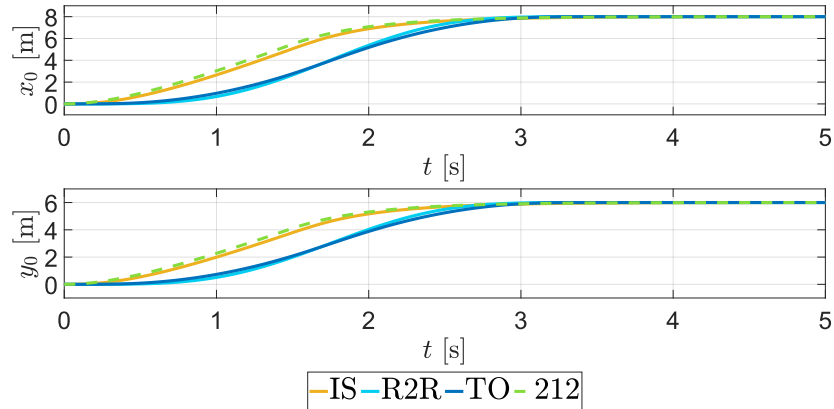


Figure 4.1: Position of container

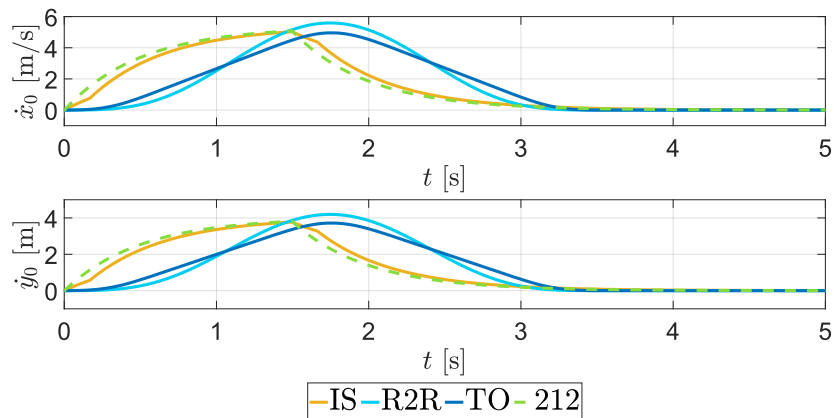


Figure 4.2: Velocity of container

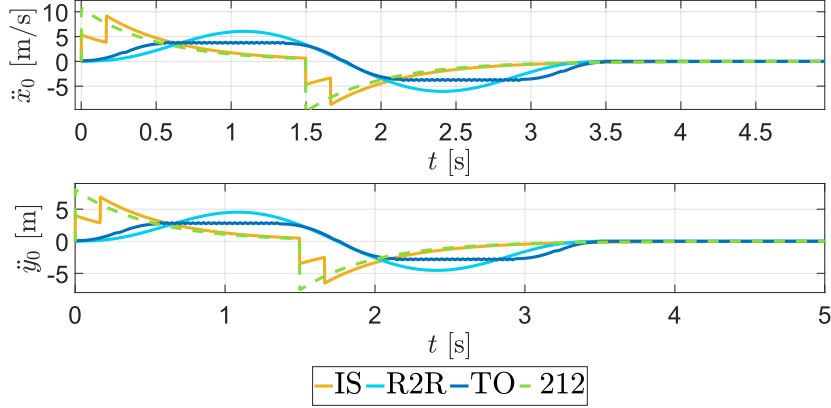


Figure 4.3: Acceleration of container

tainer at each moment in time. A noticeable point is that, although the suggested R2R and TO trajectories operate at higher velocities compared to the remaining trajectories (Fig. 4.2), their acceleration is smaller and smoother (Fig. 4.3). Con-

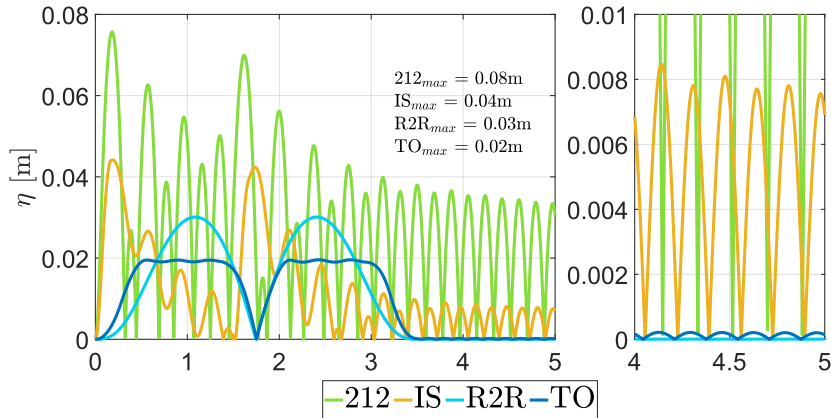


Figure 4.4: Sloshing height in open-loop control

sidering (Fig. 4.4), it is evident that the sloshing height of time optimal TO and R2R trajectories are suppressed and significantly small compared to IS and 212 trajectories. Especially the proposed TO, which have the smallest acceleration and smallest sloshing height. Although the TO trajectory could obtain smaller sloshing in the same period compared to the R2R trajectory, we can clearly see that the R2R trajectory is more robust with model error since there is no liquid oscillation in the final position.

4.2 Trajectory Feedforward experiment

The experimental setup for liquid transportation consists of a linear motion system designed to move a cylindrical container along the x-axis. The system is driven by a belt transmission and actuated by an R88D-KN04H-ECT servo drive paired with a 400 W servo motor. The motion control is implemented in velocity tracking mode, allowing precise regulation of the container's speed throughout the trajec-

tory. This setup, developed as part of my thesis, is supported and carried out at the Motion Control and Applied Robotics Laboratory. It serves as a versatile platform for studying and controlling liquid sloshing phenomena during high-speed or abrupt movements, and for validating advanced motion control algorithms. The



Figure 4.5: Experimental setup

experiment can be viewed at the following link: <https://youtu.be/5opAmY9NtqE>. In this setup, the container follows a reference position of $0 \rightarrow 800 \rightarrow 0$ mm with transporting time of 1 second and a phase distance of 800 mm each. The container has a radius of 60 mm, and the liquid height varies across experiments: 160 mm in Experiments 1 and 2, and 240 mm in Experiment 3.

Two trajectories are compared: the flatness-based rest-to-rest trajectory (defined in Equation 2.42) and a conventional 2-1-2 trajectory with a maximum acceleration of 8100 mm/s² and a maximum velocity of 900 mm/s.

As shown in the video, the flatness-based trajectory not only achieves outstanding small liquid sloshing performance compared to the 2-1-2 trajectory but also eliminates liquid oscillation at the final state, validating the correctness of the proposed method. Even under model error—such as added liquid mass—the flatness-based trajectory exhibits strong robustness, with only minor sloshing observed in the final phase.

4.3 Controller tracking performance of time optimal trajectory

In this scenario, the container embarks on a journey from its starting point at coordinates $(0, 3)$ to reach a target location specified at $(10, 2)$. The path, however, is obstructed by two rectangular obstacles lying in $\{(x,y) : 1 < x < 2, 1 < y < 5\}$ and $\{(x,y) : 1 < x < 2, 1 < y < 5\}$. In the simulation, we use the white noise in (Fig. 4.7) as the lumped disturbance that directly impacts the liquid sloshing system. The Equation 2.64 is being optimized to find an appropriate trajectory to achieve our goal. The constraint is $\eta_{n(max)} \leq 0.01$. And four of our controllers would tracking this flatness-based trajectory. As illustrated in Figures 4.8, 4.9,

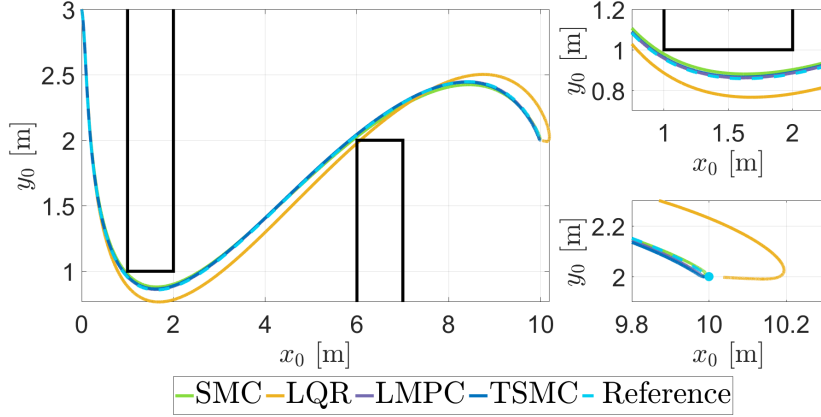


Figure 4.6: Displacement of container position along xy -axis - second scenario

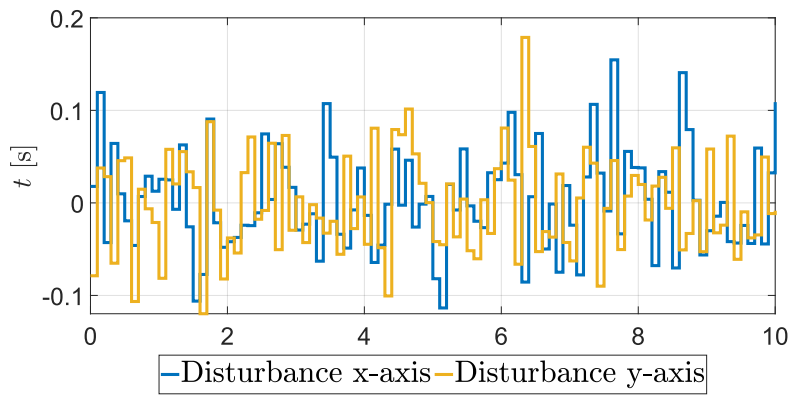


Figure 4.7: Unknown disturbance for both x-axis and y-axis

and supported by the data in Table 4.2, the TSMC outperforms the LMPC, SMC, and LQR controllers in terms of tracking accuracy. Despite minor oscillations in the maximum sloshing height caused by external disturbances, the state position \mathbf{q} under TSMC remains stable and closely follows the desired trajectory. Table 4.2 further details this comparison using four distinct performance metrics. Figures 4.10 and 4.11 show that the container's velocity remains well-regulated across all controllers, even when subjected to significant disturbances. In contrast, the sloshing mass velocity, \dot{m}_n , is noticeably affected by these disturbances. The LMPC, in particular, exhibits poor control performance for \dot{q} , highlighting one of its main limitations—its reduced effectiveness under large disturbances. Among the compared controllers, TSMC demonstrates the most effective suppression of sloshing in the final steady state. Although the TSMC has better tracking performance compared to two other controllers, there is no major difference in the control effort between them as can be seen in (Fig. 4.12). The (Fig. 4.13) represents the error estimation of immeasurable velocity \dot{q} , which is small enough. The peaks of the plot are mainly caused by the rapid change of white noise disturbance and its amplitude.

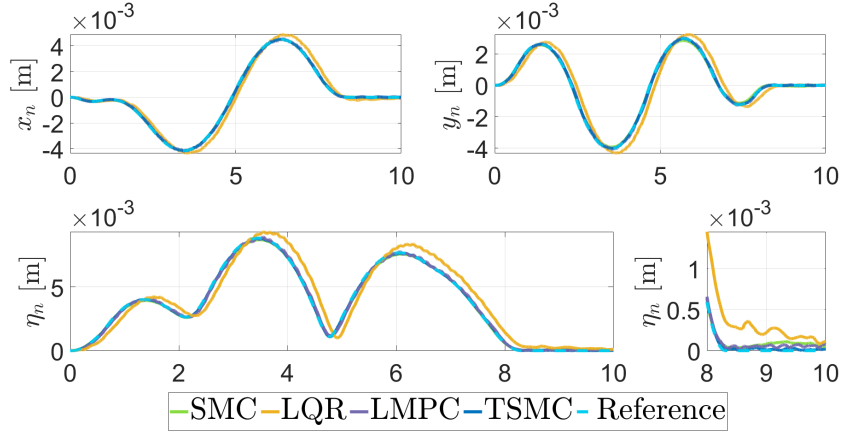


Figure 4.8: Dislplacement of sloshing mass m_n and sloshing height \dot{q} - second scenario

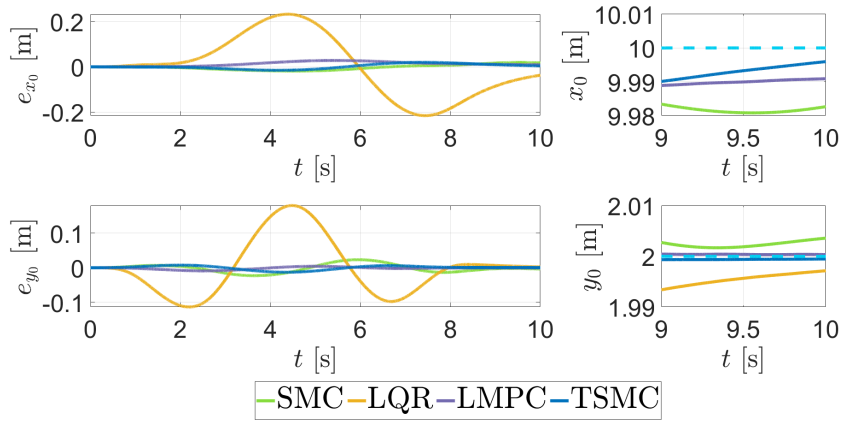


Figure 4.9: Error of container position throughout the process in a time domain - second scenario

4.4 Sloshing height constraint for rest-to-rest trajectory

To suppress sloshing during motion, we apply the Control Barrier Function (CBF) described in Section 3.3.2, along with a hard constraint in the LMPC formulation to limit the maximum sloshing height to $\eta_{\max} = 0.01$ m. In this scenario, the container moves from the initial position $(0, 3)$ to the target position $(10, 5)$, while avoiding a rectangular obstacle located within the region $\{(x, y) : 4 < x < 6, 1 < y < 7\}$. White noise (shown in Fig. 4.7) is included as a lumped disturbance throughout the simulation. To bypass the obstacle, the container is guided through the intermediate point $(3, 0)$. If we use a rest-to-rest trajectory based on flatness interpolation, the trajectory is given by:

$$\begin{aligned} y_1 &= x_i + (x_f - x_i)\tau^5(216 - 450\tau + 540\tau^2 - 315\tau^3 + 70\tau^4) \\ y_2 &= y_i + (y_f - y_i)(-5\tau_2 + 2\tau_2^2 + 4\tau_2^3) \end{aligned} \quad (4.5)$$

where $\tau = (t - t_i)/(t_f - t_i)$ and $\tau_2 = (y_1 - y_i)/(x_f - x_i)$. The resulting trajectory is illustrated in Figure 4.14: Since CBF can be implemented in real-time, they are suitable for this problem, which requires immediate response to unknown disturbances, and ensures safety constraints are continuously respected, as can be seen

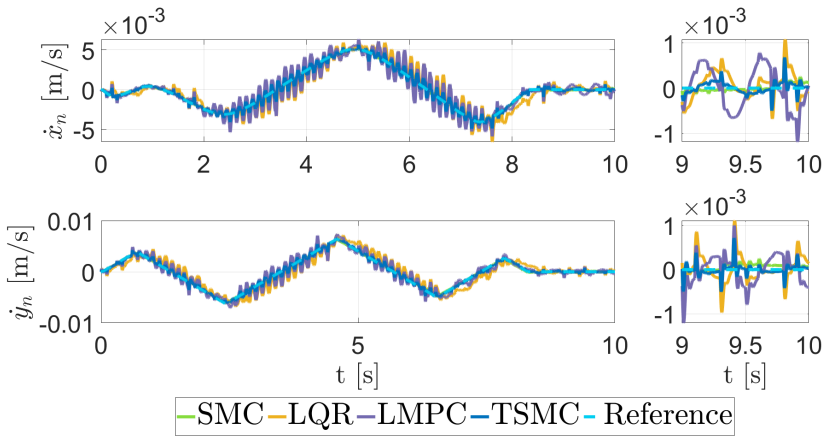


Figure 4.10: Velocity of sloshing mass m_n and velocity of container - second scenario

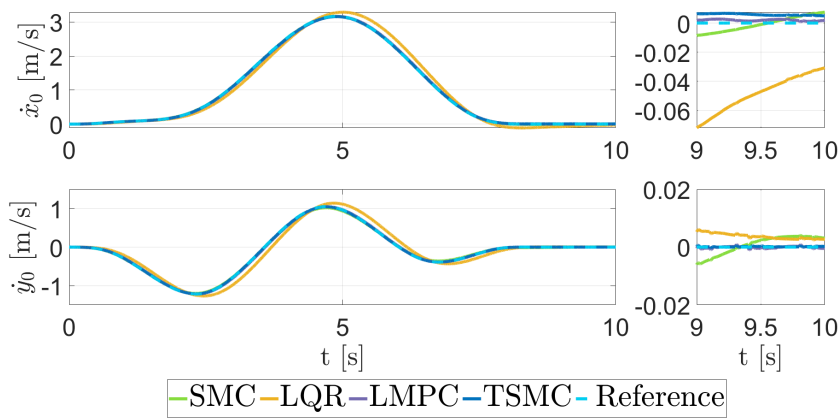


Figure 4.11: Velocity of sloshing mass m_n and velocity of container - second scenario

in (Fig 4.15). In the LMPC design, the sloshing height constraint is enforced as a hard constraint, meaning that any violation of this limit is strictly prohibited during optimization. However, there is still a small violation of the maximum sloshing height at $t = 5.2\text{s}$. To satisfy the system's safety constraints, some deviation from the desired trajectory must be allowed. Specifically, the y-axis acceleration is constrained to ensure that $\bar{\eta}n \leq \eta_{\max}$, as shown in Figure 4.19. Consequently, both the position Figure 4.16 and the velocity (Figures 4.17 and 4.14) along the y-axis deviate from the intended path. As a result, the system requires more time to reach the target position. In Table 4.3, overall, we could conclude that the proposed TSMC-CBF methods has better performance compared to LMPC. In terms of computational efficiency, Figure 4.20 presents both the execution and total simulation times. The TSMC-CBF controller significantly outperforms the LMPC, achieving an total simulation time of just 17.2 seconds compared to LMPC's 100.5 seconds. Initialization is also faster, taking only 0.7 second versus 1.8 seconds for LMPC. Moreover, the TSMC-CBF simulation consumes only 14.17 MB of memory, which is substantially lower than the 79.36 MB required by the LMPC. These results underscore the superior efficiency of the TSMC-CBF controller, making

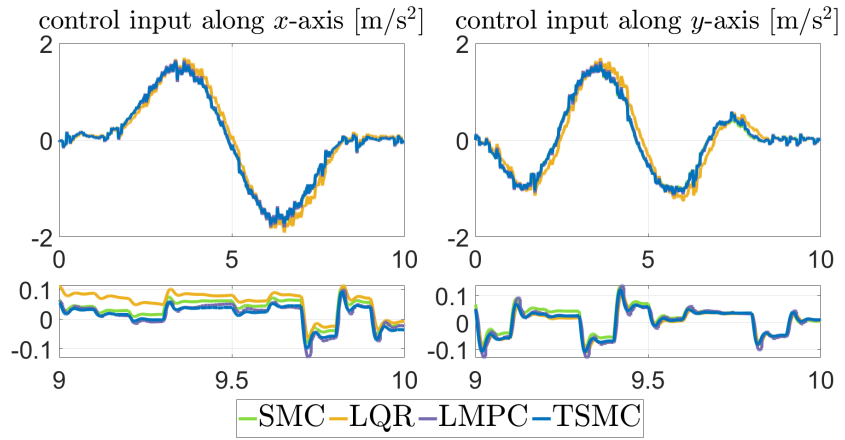


Figure 4.12: Control signal input: acceleration of container - second scenario

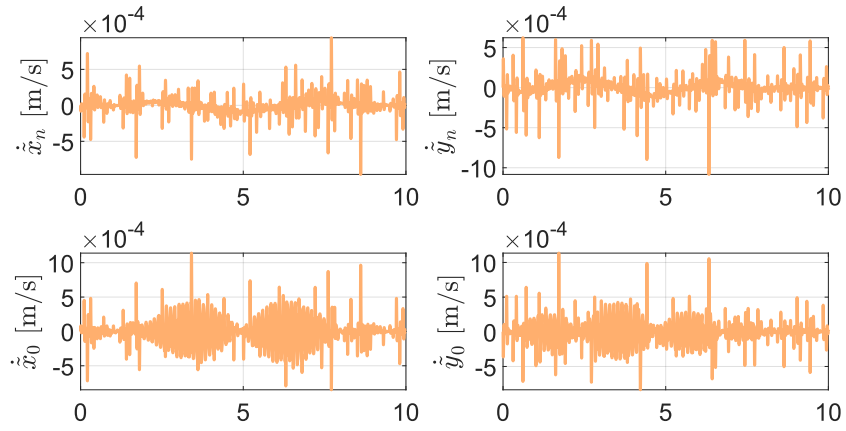


Figure 4.13: Error estimation of state variable \dot{q} - second scenario

it well-suited for applications demanding rapid computation and low resource usage. Simulations were conducted in the Simulink environment using the `ode45` solver with a variable time step configuration, on a system equipped with a Ryzen 7 5800HS CPU, 16 GB of RAM, and an NVIDIA GeForce GTX 1650 GPU.

Table 4.2: The performance index in second scenario

Output variable	Control Strategy	ISE	ITSE	IAE	ITAE
x_n	TSMC	1.0237×10^{-8}	5.0135×10^{-8}	2.5316×10^{-4}	1.2396×10^{-3}
	LMPC	4.7563×10^{-8}	2.4481×10^{-7}	5.3215×10^{-4}	2.7552×10^{-3}
	SMC	1.8276×10^{-8}	1.0545×10^{-7}	3.6282×10^{-4}	2.0273×10^{-3}
	LQR	1.4423×10^{-6}	8.1083×10^{-6}	3.0096×10^{-3}	1.6351×10^{-2}
y_n	TSMC	1.2633×10^{-8}	4.8006×10^{-8}	2.7679×10^{-4}	1.1470×10^{-3}
	LMPC	6.4814×10^{-8}	2.6302×10^{-7}	6.2686×10^{-4}	2.7018×10^{-3}
	SMC	5.4068×10^{-8}	2.7096×10^{-7}	5.9940×10^{-4}	3.0303×10^{-3}
	LQR	2.3720×10^{-6}	1.0481×10^{-5}	3.8289×10^{-3}	1.6861×10^{-2}
x_0	TSMC	1.2020×10^{-3}	7.7336×10^{-3}	8.9321×10^{-2}	5.5439×10^{-1}
	LMPC	2.5569×10^{-3}	1.5023×10^{-2}	1.2964×10^{-1}	7.8171×10^{-1}
	SMC	1.3152×10^{-3}	8.1633×10^{-3}	9.2962×10^{-2}	5.5972×10^{-1}
	LQR	1.7351×10^{-1}	$1.0074 \times 10^{+00}$	$1.0553 \times 10^{+00}$	$6.1986 \times 10^{+00}$
y_0	TSMC	3.2502×10^{-4}	1.3566×10^{-3}	4.3126×10^{-2}	1.8666×10^{-1}
	LMPC	1.4751×10^{-4}	4.3570×10^{-4}	2.6986×10^{-2}	9.7528×10^{-2}
	SMC	1.4740×10^{-3}	7.3974×10^{-3}	9.6093×10^{-2}	4.9209×10^{-1}
	LQR	6.4484×10^{-2}	2.7513×10^{-1}	5.9677×10^{-1}	$2.5986 \times 10^{+00}$

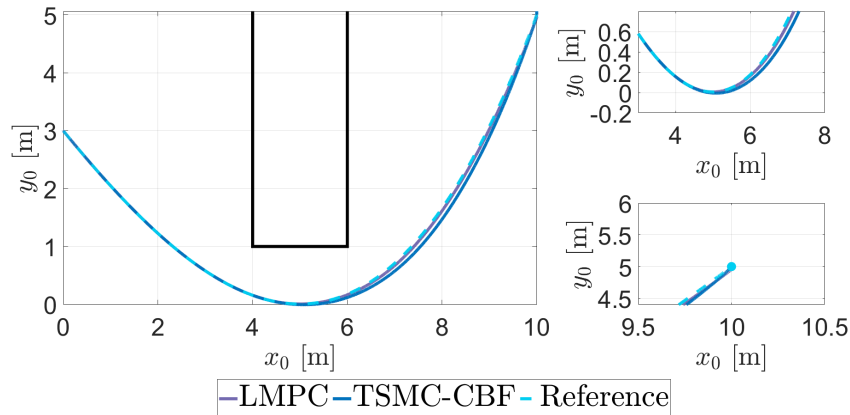


Figure 4.14: Displacement of container position along xy -axis - third scenario

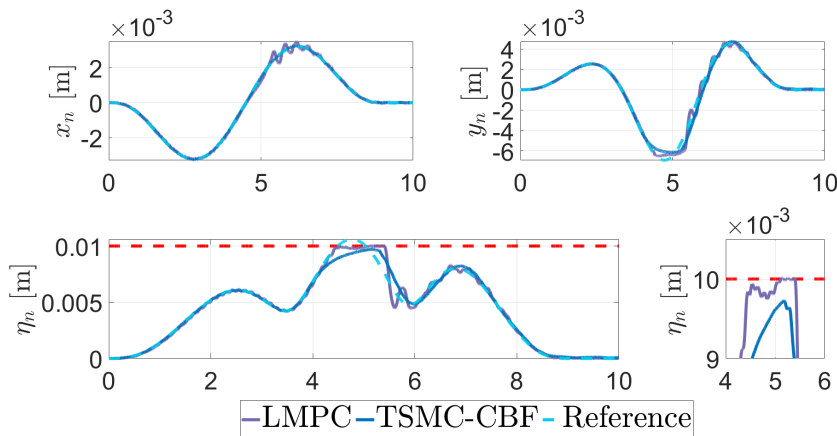


Figure 4.15: Dislplacement of sloshing mass m_n and sloshing height \dot{q} - third scenario

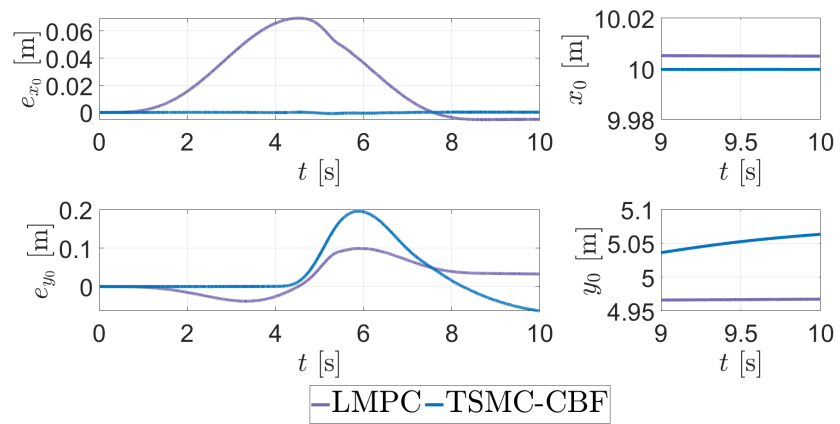


Figure 4.16: Displacement of container position throughout the process in a time domain - third scenario

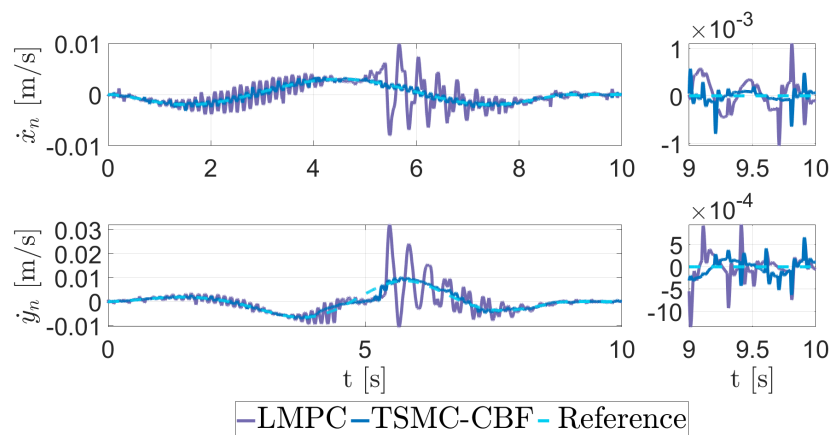


Figure 4.17: Velocity of sloshing mass m_n and velocity of container - third scenario

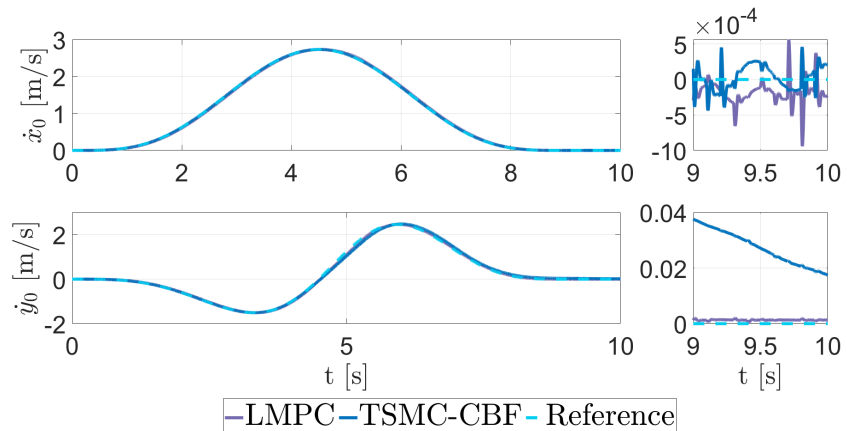


Figure 4.18: Velocity of sloshing mass m_n and velocity of container - third scenario

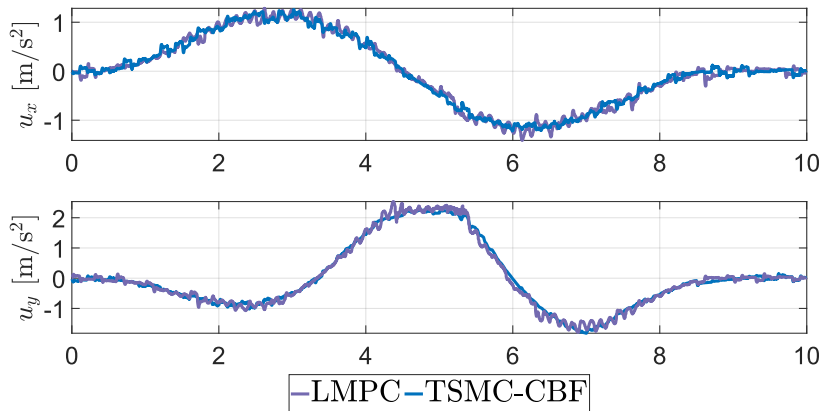


Figure 4.19: Control signal input: acceleration of container - third scenario

Table 4.3: The performance index in third scenario

Output variable	Control Strategy	ISE	ITSE	IAE	ITAE
x_n	TSMC	1.5187×10^{-9}	7.7480×10^{-9}	9.4906×10^{-5}	4.8354×10^{-4}
	LMPC	1.2278×10^{-7}	6.6849×10^{-7}	7.0036×10^{-4}	3.6212×10^{-3}
y_n	TSMC	1.0977×10^{-6}	5.9487×10^{-6}	1.8290×10^{-3}	1.0521×10^{-2}
	LMPC	8.7498×10^{-7}	4.8212×10^{-6}	1.5902×10^{-3}	8.4916×10^{-3}
x_0	TSMC	6.4100×10^{-7}	3.9084×10^{-6}	1.8202×10^{-3}	1.1304×10^{-2}
	LMPC	1.1877×10^{-2}	5.2317×10^{-2}	2.4572×10^{-1}	$1.1212 \times 10^{+00}$
y_0	TSMC	5.8822×10^{-2}	3.6575×10^{-1}	4.5705×10^{-1}	$3.0114 \times 10^{+00}$
	LMPC	2.2733×10^{-2}	1.4088×10^{-1}	3.7848×10^{-1}	$2.3157 \times 10^{+00}$

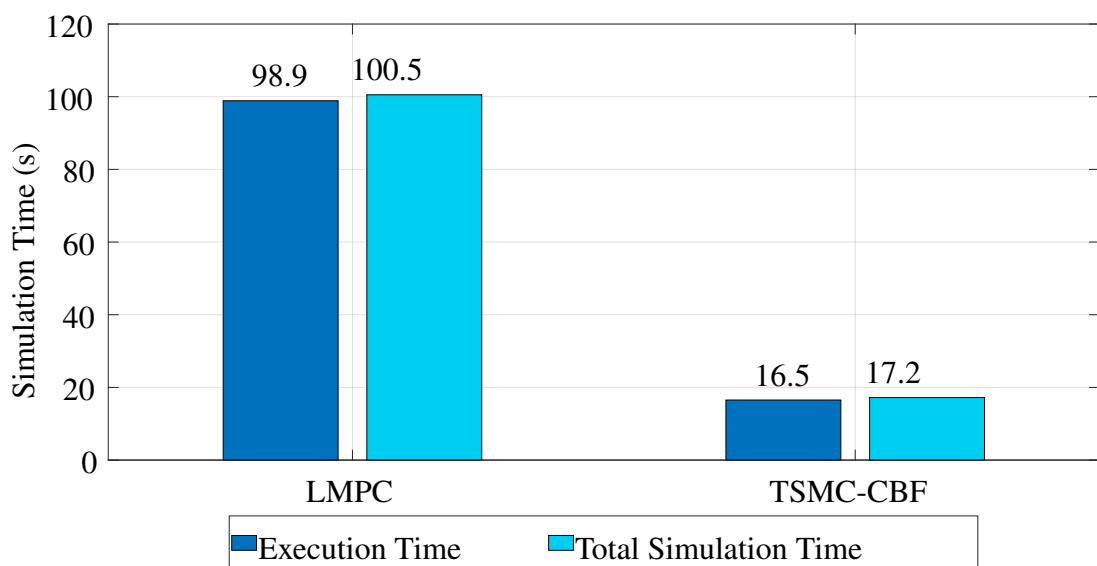


Figure 4.20: Compare controllers simulation time

CONCLUSIONS

In this comprehensive study, our exploration of the sloshing system's flat output has yielded promising insights into tackling the sloshing suppression challenge through the design of a well-suited trajectory and the proposed control methodology.

- First time introduce the approximate flat output of nonlinear mass-spring-damper system. Analyze the errors in moving in straight line, curvy 2D trajectory.
- Presenting an innovative flatness-based time-optimal avoid obstacle trajectory, that offers significant improvements in the overall performance of liquid transfer systems and the traditional rest-to-rest trajectory for simplicity.
- For the LMPC, it is enables multiple constraints if we want to manipulate more state variables, for instance sloshing height and container's velocity. And also the Lyapunov constraint guarantees the system to converge.
- To ensure effective trajectory tracking, we've proposed the utilization of the novel control strategy known as TSMC-ESO combined with CBF. The TSMC-ESO controller is designed to ensure precise tracking of the recommended trajectory and enhance precision, while the CBF meets the requirements, constraints, and reliability of the liquid transfer process.

However, there are still some disadvantages in this study

- The trajectory references are generated offline. In other words, the trajectory just suitable for the static obstacles, and its position must be known.
- Since the proposed flat output is only available for an approximate nonlinear mode. The novel flat output must be carefully evaluated before being applied in the path planning stage due to the model error depending on the sloshing height
- All the proposed algorithm are model-based methods. Therefore, it requires quite precise knowledge about the model to have the best performance.

In this study, several limitations need to be acknowledged and addressed. Firstly, the proposed work has not been validated through practical experiments, which restricts the confirmation of its real-world applicability and performance. Experimental validation is crucial to ensure that the theoretical results hold under actual conditions and account for potential unforeseen dynamics. Secondly, the control method proposed in this study requires complex calculations, which could

pose challenges for real-time implementation, especially in systems with limited computational resources or stringent timing requirements. Finally, this study does not focus on a specific physical platform, which could limit its direct application to existing systems. The control methodology assumes that acceleration serves as the control signal, a simplification that may not align with the constraints or configurations of all practical systems.

While my theoretical groundwork is robust, the numerical simulation is to validate my method in terms of control response, safe constraints, time optimization, and obstacle avoidance. However, the next crucial step is to validate our findings through practical experiments to confirm the real-world applicability and efficacy.

RELATED PUBLICATIONS

Awards

- Third prize in the University-Level Student Scientific Research Award 2023-2024 (HUST).
- Second prize in the University-Level Student Scientific Research Award 2024-2025 (HUST).

Related publications

- 1 **Khanh Nguyen Viet**, Hue Luu Thi, Thanh Cao Duc1, Huy Nguyen Danh, Minh Nhat Vu, and Tung Lam Nguyen Time-optimal motion planning and anti-sloshing control for a container under disturbances, IEEE Access (**SCIE Q1 Scopus**, doi.org/10.1109/ACCESS.2025.3533541)
- 2 **Khanh Nguyen Viet**, Minh Do Duc, Thanh Cao Duc and Lam Nguyen Tung "Anti-sloshing control: Flatness-based trajectory planning and tracking control with an integrated extended state observer", IET Cyber-Systems and Robotics (**Q3 Scopus**,doi.org/10.1049/csy2.12121)
- 3 **Viet Khanh Nguyen**, Hue Luu Thi, Duc Thanh Cao, Dang Huu Bang, and Tung Lam Nguyen "The Non-Flatness Property of the Liquid Sloshing System and an Approximate Approach" 2024 International Conference on Advanced Technologies for Communications Program (doi.org/10.1109/ATC63255.2024.10908250)
- 4 **Khanh Nguyen Viet**, Hue Luu Thi, Minh Do Duc, Thanh Cao Duc, Huy Nguyen Danh, and Nguyen Tung Lam "Input Shaping Integrated With Lyapunov Based Model Predictive Control For Anti-Sloshing Problem" 2024 3rd International Conference on Advances in Information and Communication Technology (**Q4 Scopus**, doi.org/10.1007/978-3-031-80943-9_94)
- 5 **Viet Khanh Nguyen**, Hue Luu Thi, Duc Thanh Cao, Tung Lam Nguyen, Duc Minh Do and Thanh Ha Vo "Control Strategy for Liquid Transfer Using a Four-wheel Mecanum Mobile Robot Platform" The 9th International Conference on Applying New Technology in Green Buildings (doi.org/10.1109/ATiGB63471.2024.10717655)
- 6 Minh Do Duc, **Khanh Nguyen Viet**, Thanh Cao Duc, Ho Thanh Hieu, Duc Duong Minh and Lam Nguyen Tung "Flatness-based non-linear control for path planning and tracking of sloshing liquid container", Journal of Science and Technology, pp. 41–28, June 2023 (doi.org/10.51316/jst.168.ssad.2023.33.3.6)

- 7 Cao Đức Thanh, **Nguyễn Việt Khanh**, Trần Thị Thanh Thảo, Nguyễn Văn Minh, Nguyễn Danh Huy, Nguyễn Tùng Lâm "Kiểm soát dao động của chất lỏng chuyển động theo phương nằm ngang bằng cách tạo quỹ đạo dựa trên tính phẳng", *Journal of Military Science and Technology* (doi.org/10.54939/1859-1043.j.mst.FEE.2024.92-98)
- 8 Thanh Cao Duc, **Khanh Nguyen Viet**, Minh Do Duc and Lam Nguyen Tung "Flatness-based nonlinear approach to liquid sloshing in a 2-D moving container", *Vietnam International Conference and Exhibition on Control and Automation (VCCA) 2024 (Accepted)*

BIBLIOGRAPHY

- [1] A. Alshaya and A. Alshayji, “Robust multi-steps input command for liquid sloshing control,” *Journal of Vibration and Control*, vol. 28, p. 2607–2624, May 2021.
- [2] M. Arafa, “Finite element analysis of sloshing in rectangular liquid-filled tanks,” *Journal of Vibration and Control*, vol. 13, p. 883–903, July 2007.
- [3] M. Luo, A. Khayyer, and P. Lin, “Particle methods in ocean and coastal engineering,” *Applied Ocean Research*, vol. 114, p. 102734, Sept. 2021.
- [4] H. Li, X. Zhang, and X. Yang, “Numerical study of liquid sloshing using smoothed particle hydrodynamics with adaptive spatial resolution,” *Engineering Analysis with Boundary Elements*, vol. 159, p. 272–287, Feb. 2024.
- [5] R. A. Ibrahim, *Liquid Sloshing Dynamics*. Cambridge University Press, May 2005.
- [6] W. Aribowo, T. Yamashita, K. Terashima, and H. Kitagawa, “Input shaping control to suppress sloshing on liquid container transfer using multi-joint robot arm,” in *2010 IEEE/RSJ International Conference on Intelligent Robots and Systems*, p. 3489–3494, IEEE, Oct. 2010.
- [7] Y. Baozeng and Z. Lemei, “Hybrid control of liquid-filled spacecraft maneuvers by dynamic inversion and input shaping,” *AIAA Journal*, vol. 52, p. 618–626, Mar. 2014.
- [8] L. Guagliumi, A. Berti, E. Monti, and M. Carricato, “A simple model-based method for sloshing estimation in liquid transfer in automatic machines,” *IEEE Access*, vol. 9, pp. 129347–129357, 2021.
- [9] R. Di Leva, M. Carricato, H. Gatringer, and A. Müller, “Sloshing dynamics estimation for liquid-filled containers performing 3-dimensional motions: modeling and experimental validation,” *Multibody System Dynamics*, vol. 56, p. 153–171, Aug. 2022.
- [10] B. Pridgen, K. Bai, and W. Singhose, “Slosh suppression by robust input shaping,” in *49th IEEE Conference on Decision and Control (CDC)*, p. 2316–2321, IEEE, Dec. 2010.
- [11] M. Grundelius and B. Bernhardsson, “Motion control of open containers with slosh constraints,” *IFAC Proceedings Volumes*, vol. 32, p. 6142–6147, July 1999.

- [12] G. Rigatos, M. Abbaszadeh, and M. A. Hamida, “Nonlinear optimal control for the dynamics of the underactuated slosh-container system,” *Ships and Offshore Structures*, vol. 17, p. 1901–1915, July 2021.
- [13] R. I. C. Muchacho, R. Laha, L. F. Figueiredo, and S. Haddadin, “A solution to slosh-free robot trajectory optimization,” in *2022 IEEE/RSJ International Conference on Intelligent Robots and Systems (IROS)*, p. 223–230, IEEE, Oct. 2022.
- [14] R. D. Leva, M. Carricato, H. Gattringer, and A. Muller, “Time-optimal trajectory planning for anti-sloshing 2-dimensional motions of an industrial robot,” in *2021 20th International Conference on Advanced Robotics (ICAR)*, IEEE, Dec. 2021.
- [15] J. Levine, *Analysis and Control of Nonlinear Systems*. Springer Berlin Heidelberg, 2009.
- [16] L. Rothenbuchner, C. Neudorfer, M. Fallmann, F. Toth, A. Schirrer, C. Hametner, and S. Jakubek, “Efficient feedforward sloshing suppression strategy for liquid transport,” *Journal of Sound and Vibration*, vol. 590, p. 118542, Nov. 2024.
- [17] J. Lévine and D. Nguyen, “Flat output characterization for linear systems using polynomial matrices,” *Systems & Control Letters*, vol. 48, no. 1, pp. 69–75, 2003.
- [18] K. N. Viet, M. D. Duc, T. C. Duc, and T. L. Nguyen, “Anti-sloshing control: Flatness-based trajectory planning and tracking control with an integrated extended state observer,” *IET Cyber-Systems and Robotics*, vol. 6, Aug. 2024.
- [19] K. Nguyen Viet, H. Luu Thi, T. Cao Duc, H. Nguyen Danh, M. N. Vu, and T. Lam Nguyen, “Time-optimal motion planning and anti-sloshing control for a container under disturbances,” *IEEE Access*, vol. 13, p. 26707–26726, 2025.
- [20] M. FLIESS, J. LÉVINE, P. MARTIN, and P. ROUCHON, “Flatness and defect of non-linear systems: introductory theory and examples,” *International Journal of Control*, vol. 61, pp. 1327–1361, June 1995.
- [21] M. Fliess, J. Levine, P. Martin, and P. Rouchon, “A lie-backlund approach to equivalence and flatness of nonlinear systems,” *IEEE Transactions on Automatic Control*, vol. 44, pp. 922–937, May 1999.
- [22] C. Edwards and S. Spurgeon, *Sliding Mode Control*. CRC Press, Aug. 1998.

- [23] R. DeCarlo, S. Zak, and G. Matthews, “Variable structure control of nonlinear multivariable systems: a tutorial,” *Proceedings of the IEEE*, vol. 76, pp. 212–232, Mar. 1988.
- [24] S. Kurode, S. K. Spurgeon, B. Bandyopadhyay, and P. S. Gandhi, “Sliding mode control for slosh-free motion using a nonlinear sliding surface,” *IEEE/ASME Transactions on Mechatronics*, vol. 18, p. 714–724, Apr. 2013.
- [25] A. Ahmed, R. Ahmad, A. Yahya, H. H. Tahir, and J. Quinlan, “Variable structure system with sliding mode controller,” *Procedia Engineering*, vol. 53, p. 441–452, 2013.
- [26] A. D. Ames, J. W. Grizzle, and P. Tabuada, “Control barrier function based quadratic programs with application to adaptive cruise control,” in *53rd IEEE Conference on Decision and Control*, IEEE, Dec. 2014.
- [27] M. Navabi, A. Davoodi, and M. Reyhanoglu, “Optimum fuzzy sliding mode control of fuel sloshing in a spacecraft using pso algorithm,” *Acta Astronautica*, vol. 167, p. 331–342, Feb. 2020.
- [28] M. A. Al-Mashhadani, “Modeling and adaptive robust wavelet control for a liquid container system under slosh and uncertainty,” *Measurement and Control*, vol. 53, p. 1643–1653, Sept. 2020.
- [29] H. F. BAUER, “Nonlinear mechanical model for the description of propellant sloshing,” *AIAA Journal*, vol. 4, pp. 1662–1668, Sept. 1966.
- [30] L. Guagliumi, A. Berti, E. Monti, and M. Carricato, “A simple model-based method for sloshing estimation in liquid transfer in automatic machines,” *IEEE Access*, vol. 9, pp. 129347–129357, 2021.
- [31] R. D. Leva, M. Carricato, H. Gattringer, and A. Müller, “Sloshing dynamics estimation for liquid-filled containers under 2-dimensional excitation,” in *Proceedings of the 10th ECCOMAS Thematic Conference on MULTIBODY DYNAMICS*, Budapest University of Technology and Economics, 2021.
- [32] P. Mullhaupt, B. Srinivasan, J. Levine, and D. Bonvin, “Control of the toy-copter using a flat approximation,” *IEEE Transactions on Control Systems Technology*, vol. 16, p. 882–896, Sept. 2008.
- [33] B.-Z. Guo and Z.-l. Zhao, “On the convergence of an extended state observer for nonlinear systems with uncertainty,” *Systems & Control Letters*, vol. 60, p. 420–430, June 2011.

- [34] Z.-H. Wu and B.-Z. Guo, “Extended state observer for mimo nonlinear systems with stochastic uncertainties,” *International Journal of Control*, vol. 93, p. 424–436, June 2018.
- [35] S. P. Bhat and D. S. Bernstein, “Finite-time stability of continuous autonomous systems,” *SIAM Journal on Control and Optimization*, vol. 38, p. 751–766, Jan. 2000.
- [36] A. D. Ames, X. Xu, J. W. Grizzle, and P. Tabuada, “Control barrier function based quadratic programs for safety critical systems,” *IEEE Transactions on Automatic Control*, vol. 62, p. 3861–3876, Aug. 2017.
- [37] C. I. G. Chinelato, G. P. D. Neves, and B. A. Angélico, “Safe control of a reaction wheel pendulum using control barrier function,” *IEEE Access*, vol. 8, pp. 160315–160324, 2020.
- [38] H. Wang, J. Peng, F. Zhang, and Y. Wang, “A composite control framework of safety satisfaction and uncertainties compensation for constrained time-varying nonlinear mimo systems,” *IEEE Transactions on Systems, Man, and Cybernetics: Systems*, vol. 53, p. 7864–7875, Dec. 2023.